Supplementary Information

Thermally Engineered Multilevel Hybrid Encryption Device with Dynamic Erasure and Ultra-High Data Concealment Capacity

Srijeeta Biswas, Renu Raman Sahu, Omkar Deokinandan Nayak Shinkre, Shubham Meena, Ramnishanth ,Mark Vailshery, Tapajyoti Das Gupta*

Laboratory of Advanced nanostructures for Photonics and Electronics, Department of Instrumentation and Applied physics, Indian Institute of Science, C.V. Raman Road, Bengaluru-560012, India

E-mail: tapajyoti@iisc.ac.in

TABLE OF CONTENTS

1. METHODS

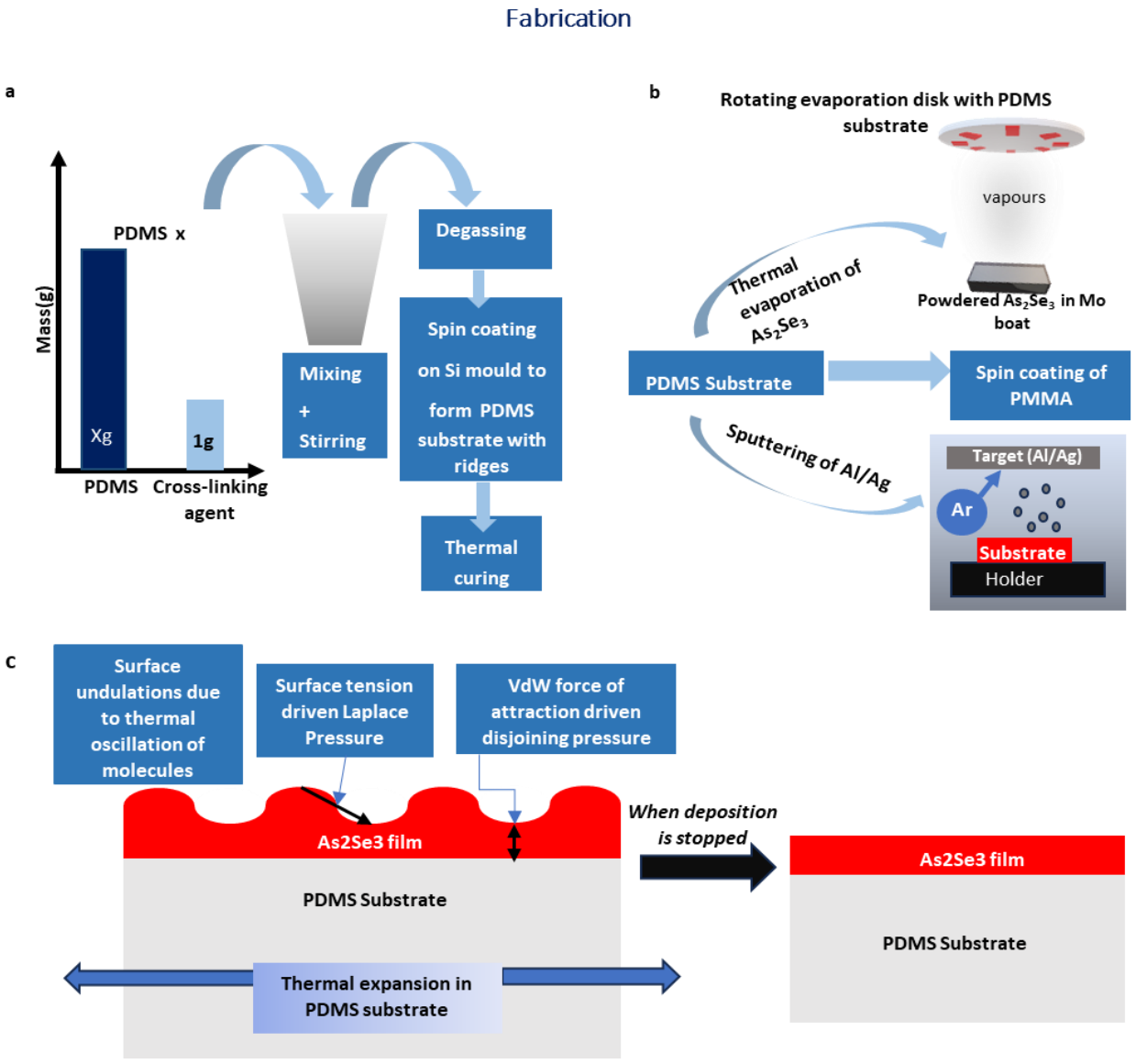

Figure 1| Schematics for sample preparation and thin film formation. *a, Fabrication of PDMS substrates of different ratios. b, Various methods of deposition of thin films on a PDMS substrate. c, Mechanism of the formation of thin uniform films on a substrate*

1.1 Preparation of PDMS

Soft and flexible Polydimethylsiloxane (PDMS) substrates are prepared by mixing X part of liquid PDMS base (Sylgard 184, Dow Corning) with 1 part of curing agent in weight ratio to form PDMSx. Substrate softness increases with an increase in the proportion of the liquid PDMS base i.e. PDMS 10 is softer than PDMS 5 which is again softer than PDMS 3 and so on. The mixture is stirred thoroughly and desiccated to remove all bubbles. The solution is then poured onto Si moulds (containing grooves pre-etched through photolithography and RIE-F) and cured at 80°C for 3 hours. Then the cured PDMS substrate (containing ridges) is peeled off from the Si mould (SI Fig.1a).

1.2 Selection of thin film and substrate materials

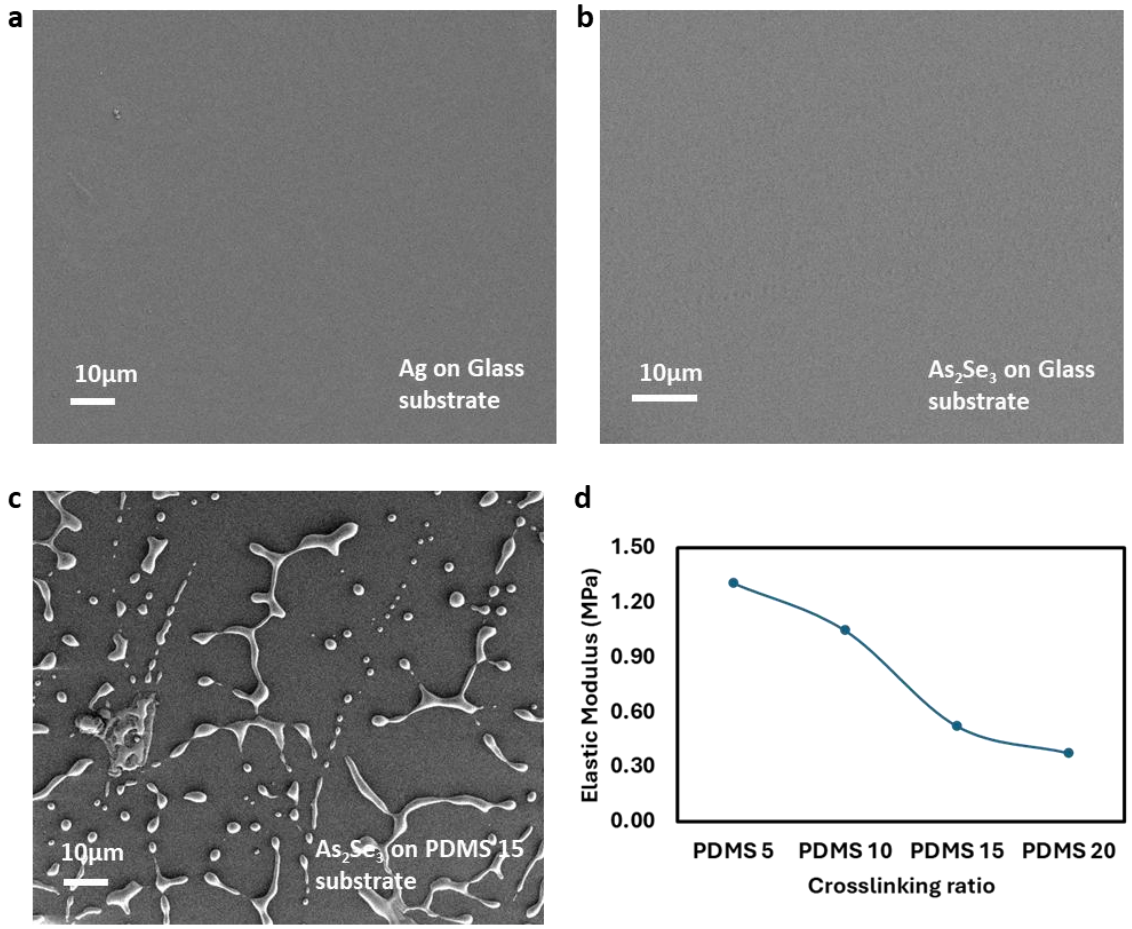

Figure 2| *a-b, Absence of wrinkles on rigid substrate (glass). c, Absence of wrinkles on very soft substrate (PDMS 15) due to dewetting. d, Elastic modulus vs. cross-linking ratio of PDMS substrates cured at* 80°C *for 3 hours.*

To achieve well-ordered wrinkles, the substrate's thermal expansion coefficient needs to be carefully balanced. It shouldn't expand excessively when heated, risking cracks in the thin film above as seen with

PDMS 15 and PDMS 20 as substrates. Young's modulus being inversely proportional to the thermal expansion coefficient, the thermal expansion coefficient of PDMS 5 and 15 can be calculated through simple ratio proportion method. The thermal expansion coefficient of PDMS 10 is $\approx 270 \times 10^{-6}/K$ and from SI Fig. 2d we see that its Young's modulus is $1.05\ MPa$. The thermal expansion coefficient of PDMS 15, having a Young's modulus of $0.53\ MPa, is \approx 535 \times 10^{-6}/K$ and that of PDMS 5, having a Young's modulus of $1.31\ MPa$, is $\approx 216 \times 10^{-6}/K$. The substrate also shouldn't contract too less during cooling, failing to provide enough stress for the thin film atop it to form uniform wrinkles, as seen with solid substrates like glass and silicon. Thus, PDMS 3, PDMS 5 and PDMS 10 are found to be the best suited for our process, their thermal expansion coefficient being in the range $200 - 350 \times 10^{-6}/K$ [1]

The thin film's thermal expansion coefficient ought to be significantly lower than that of the substrate. This ensures that during cooling, the film contracts much less than the substrate, subjecting it to substantial compressive stress, surpassing its critical stress threshold, induced by the substrate.

Thin film material	Thermal expansion coefficient	Surface energy	Young's modulus
As_2Se_3	$20 - 90 \times 10^{-6}/K$ [2–4]	$0.2J/m^2$)[5]	$1 \times 10^{10}Pa$ [4]
Al	$18 - 30 \times 10^{-6}/K$ [6]	$0.06 - 0.07J/m^2$[7]	$4 - 7 \times 10^{10}Pa$ [8]
Ag	$19 - 31 \times 10^{-6}/K$ [9]	$0.045 - 0.059J/m^2$ [10]	$3 - 8 \times 10^{10}Pa$ [11]
PMMA	$40 - 90 \times 10^{-6}/K$ [12]	$0.0377 - 0.0588J/m^2$ [13]	$3 - 4 \times 10^{9}Pa$

Table 1 | *Thermal expansion coefficient, surface energy and Young's modulus of the thin film materials used.*

The wavelength of the wrinkles formed is inversely proportional to the surface energy of the thin film. As_2Se_3 having much higher surface energy than that of Al and Ag, forms wrinkles of much smaller wavelength than the others. The Al and Ag films easily form oxides and turn yellowish when exposed to ambient atmosphere. This oxide formation is reduced significantly by curing the PDMS substrates at 80°C for more than 24 hours.

Moreover, the melting point or the glass transition temperature of the substrates and the thin films must be greater than our maximum working temperature ($i.e. > \approx 200$°C).

As_2Se_3 has generated the most well-organized 1D and 2D sinusoidal wrinkles.

1.3 Preparation of As_2Se_3 (chalcogenide) thin film

Powdered As_2Se_3 is thermally evaporated (HHV thermal evaporator) and deposited onto the PDMS substrates to form thin films. The thickness of the film and the temperature of the substrate are monitored by the respective inbuilt thickness and temperature monitoring sensors. The films are deposited at a rate of 2.5 Å/s. The substrates are kept at room temperature (SI Fig. 1b).

1.4 Preparation of Ag and Al (metals) thin films

The deposition of the metallic thin films is done by using direct current (DC) magnetron sputtering deposition technique (HHV sputtering tool). The film thickness deposited in a given time is measured through optical profilometry and the sputtering tool is accordingly calibrated to give the required film thickness. The depositions are carried out at room temperature (SI Fig. 1b). Al depositions are done at 6×10^{-3} Argon pressure and 16W sputtering power. Ag depositions are done at 9×10^{-3} Argon pressure and 16W sputtering power.

1.5 Requirements and explanation for the formation of uniform thin films

When the film deposition initiates, surface undulations occur in the film due to the thermal oscillation of the molecules. The Vander Waal's force of attraction driven disjoining pressure favours these undulations whereas the surface tension driven Laplace pressure tries to homogenize the film. Beyond a critical film thickness (which varies from material to material depending on its Vander Waal's force of attraction), the Laplace pressure predominates over the disjoining pressure and a uniform thin film is formed on the substrate. Below this critical thickness uniform film depositions do not occur. This critical thickness for As_2Se_3 is considerably higher ($\approx 60 - 70nm$) as compared to materials like Al or Ag, where uniform thin films can be achieved at much lower thicknesses ($\approx 10 - 15nm$) (SI Fig. 1c).

During the deposition the substrate is constantly struck by the hot molecules of the thin film due to which it expands. If the substrate is soft enough (i.e. having a high thermal expansion coefficient) it may form cracks, thereby cracking the thin film deposited over it. The higher the time of deposition more the chances of crack formation. To prevent this, the substrate should have an optimum softness, and the rate of deposition must be high enough so that the duration of deposition decreases.

1.6 Preparation of PMMA (polymer) thin film

495PMMA A2 resist is spin coated on the PDMS substrate at 4000 rpm for 40 seconds followed by hard baking at $110℃$ for 2 minutes to form a thin film on the substrate.

2. MATHEMATICAL MODELING OF WRINKLED THIN FILM FORMATION ON PDMS SUBSTRATES

In this section we hypothesize the wrinkle forming mechanism in rigid thin films deposited atop soft flexible substrates. Also, we propose a Wavelength Equation, and a Critical Length Equation based on a few assumptions to model the attributes of the experimentally observed wrinkles.

2.1 Thermal processing and explanation of stress formation

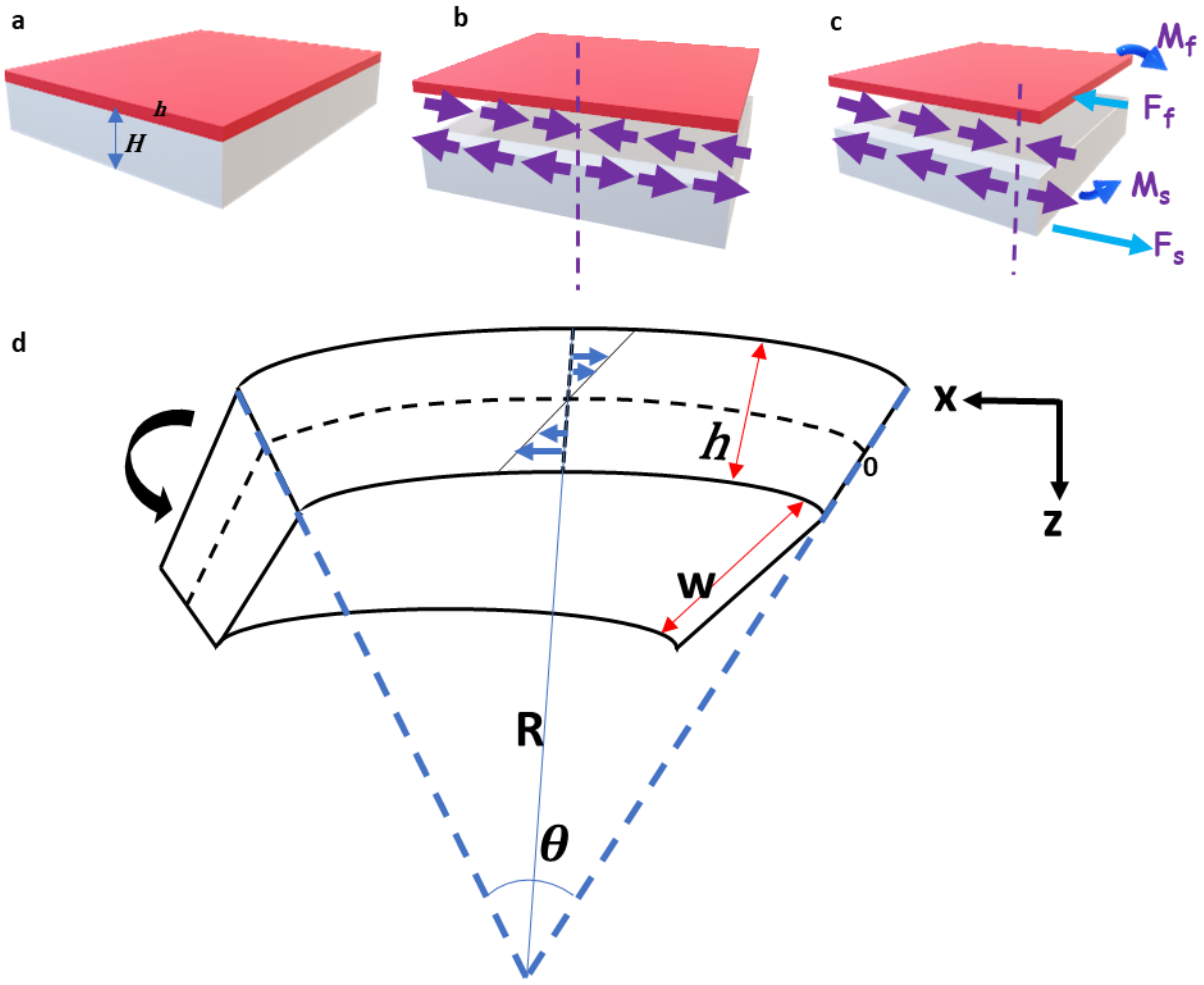

Figure 3|Stress formation mechanism in a film *a, Schematic of a film-substrate bilayer system with film thickness h and substrate thickness H. b, Schematic of the stress formation in the film and the substrate during cooling. Purple arrows indicate the direction of stress. c, Schematic representing the resultant stress and moment acting on the film and the substrate. d, Schematic showing the stress formation on the film of width w and radius of curvature R, due to the compressive stress acting over it*

When the film-substrate bilayer system as shown in SI Fig.3a starts cooling down, the PDMS substrate, owing to its higher thermal expansion coefficient than that of the film deposited atop, contracts faster than the film. In order to maintain the compatibility between the film and the substrate, the substrate experiences a tensile stress whereas the film experiences a compressive stress (depicted in SI Fig. 3b). In SI Fig. 3c we have replaced the interfacial set of stresses by a single force and moment for each of the film and the substrate, F_f and M_f for the film and F_s and M_s for the substrate. The system will bend to counteract the unbalanced moments. Considering the film to be a longitudinal beam and defining the strain over it as, (SI Fig. 3d)

$$Strain = \frac{\{R\theta-(R-h)\theta\}}{R\theta} \quad (1)$$

Therefore, the stress acting over it is defined as,

$$\sigma_f = \frac{Y_f\{R\theta-(R-h)\theta\}}{R\theta}$$

$$\Longrightarrow \sigma_f = \frac{Y_f h}{R} \quad (2)$$

Where σ_f is the stress acting on the film, Y_f is its Young's modulus, R is the radius of curvature, θ is the angle of curvature and h is the film thickness. Thus, we can see that for a given film stiffness and radius of curvature, higher the film thickness higher is the stress experienced by it. This is the reason why we get wrinkles of larger wavelengths for higher film thicknesses and wrinkle formation also becomes easier with increase in film thickness.

2.2 Hypothesis of wrinkle formation mechanism and our proposed Wavelength Equation

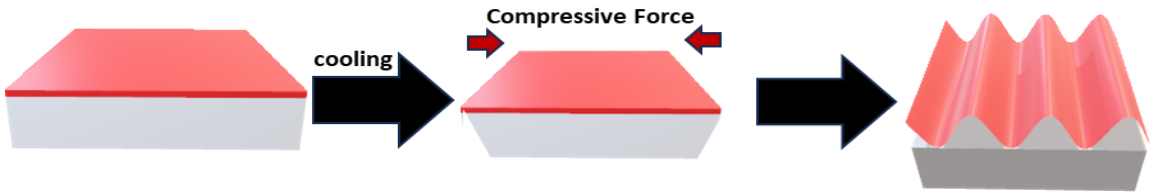

Figure 4|Schematic showing the wrinkle formation mechanism in the thin film. *Due to the mismatch in the thermal expansion coefficient of the film and the substrate, during cooling, wrinkles are formed in the film to maintain the equilibrium of the system.*

When the system is heated, the substrate expands more than the film, thereby exerting a tensile stress over the film. If the substrate expansion is too high, as in the case of PDMS 15,20 and above, the tensile stress acting on the film is so high that cracks are formed in it (SI Fig.2c).

As the system cools, the substrate contracts more than the film, resulting in a compressive stress on the film. To maintain equilibrium, wrinkles with appropriate wavelength form in the film, as shown in SI Fig.4 The size of these wrinkles directly correlates with the stress on the film. A greater mismatch in thermal expansion coefficients between the film and substrate leads to increased stress on the film, resulting in wrinkles with larger wavelength. Similarly, cooling the system from a higher temperature increases the stress on the film, again enlarging the wrinkles' wavelength.

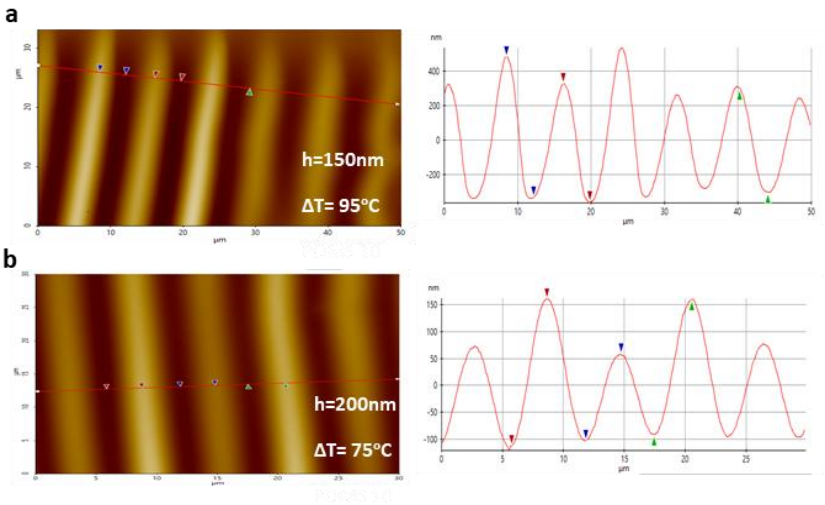

Cursor	Δx(μm)	Δy(nm)
Red	3.633	690.164
Green	3.865	604.846
Blue	3.668	816.852

Cursor	Δx(μm)	Δy(nm)
Red	2.900	272.959
Green	3.096	252.585
Blue	2.900	159.937

Figure 5|AFM images illustrating that the wavelength of the wrinkles is much greater than their amplitude. *Samples having a film of As_2Se_3 deposited over PDMS 5 substrate. The line plot shows the surface profile of the film across the line drawn over the AFM image. The table to the right gives the Δx(μm) and Δy(nm) values of the cursor pairs in the line profile. Δx(μm) is half of the wavelength of the wrinkles whereas Δy(nm) is their amplitude. a, for a film thickness of 150nm, and change is temperature of 95°C, the wavelength and amplitude of the wrinkles are around 7.5μm and 700nm respectively. b, for a film thickness of 200nm, and change is temperature of 75°C, the wavelength and amplitude of the wrinkles are around 6μm and 200nm respectively. Thus, the amplitude of the wrinkles is much smaller than their wavelengths.*

MATHEMATICAL MODELING

Let us consider that stress energy U leads to the formation of n number of wrinkles

$$U = \int_0^U dU$$

$$= \int_0^l f\,dx$$

Where f is the compressive force acting on the film at an instant and dx is the contraction in the film along the direction of the compressive force at that instant. l is the total contraction that should occur in the film due to the total stress energy U.

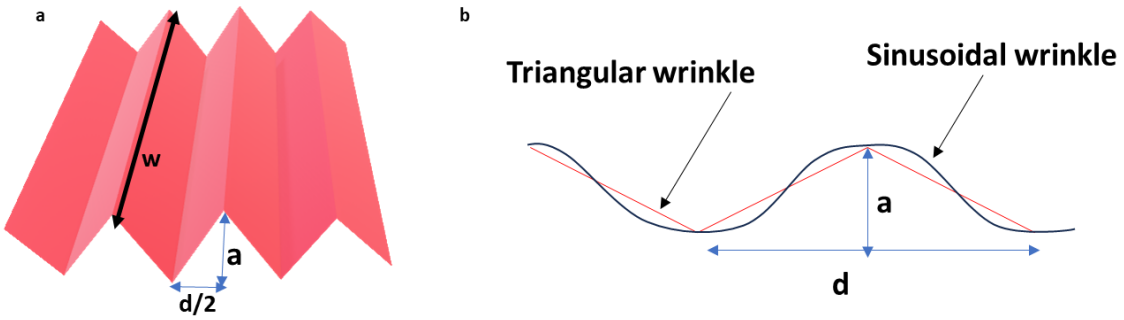

Figure 6| Schematic of an array of wrinkles*. a, Width w, amplitude a, and periodicity (wavelength) d. For modeling purpose, we have assumed the wrinkles to be triangular. b, Schematic representing the superposition of sinusoidal and triangular wrinkles of same amplitude and wavelength. Sinusoidal wrinkles have higher surface are than triangular ones.*

The Young's modulus of a system is defined as

$$Y = \frac{\sigma}{\epsilon}$$

Where Y is the Young's modulus of the system, σ is the stress and $\in$ is the strain acting on it. The strain acting on the film in the bilayer system can be defined as

$$\in = (\alpha_s - \alpha_f)Y_f$$

Where Y_f is the Young's modulus of the film, α_s and α_f are the thermal expansion coefficients of the substrate and the film, respectively.

Thus, the compressive force f acting on the film at an instant is defined as

$$f = Y_f(\alpha_s - \alpha_f)\Delta T wh \quad (3)$$

ΔT signifies the temperature change within system and w, h are the width and thickness of the film, respectively. Therefore, the stress energy U can be defined as

$$U = \int_0^l Y_f(\alpha_s - \alpha_f)\,\Delta T(wh)dx$$

$$= Y_f(\alpha_s - \alpha_f)\Delta T whl \quad (4)$$

Total surface area of a triangular wrinkle can be defined as (assuming triangular wrinkles as shown in SI Fig.6a, and using Pythagoras theorem,)

$$A = 2 \times 2w\sqrt{\frac{d^2}{4} + a^2}$$

Therefore, the surface area of a sinusoidal wrinkle will be defined as

$$A = C \times 2 \times 2w\sqrt{\frac{d^2}{4} + a^2} \quad (5)$$

Where a is the amplitude and d is the periodicity(wavelength) of the wrinkle. The first 2 is for the top and the bottom surface of the wrinkle and the second 2 is for both the faces of the triangle. Only the bottom surface of the wrinkle is the newly formed surface during wrinkle formation. C is a proportionality constant, greater than 1, which accounts for the disparity in surface area between a sinusoidal and a triangular wrinkle. The surface area of a sinusoidal wrinkle is greater than that of a triangular wrinkle as shown in SI Fig.6b. Higher the value of the amplitude and periodicity of the wrinkles, higher is the value of C.

At the verge of wrinkle formation, the stress energy gets converted to the surface energy of the newly formed surfaces of the wrinkles. Thus, from energy conservation we get

$$Y_f(\alpha_s - \alpha_f)\Delta T whl = Cn2w\sqrt{\frac{d^2}{4} + a^2}\gamma_f \quad (6)$$

Where γ_f is the surface energy of the thin film.

Now, since $d \gg a$ (refer SI Fig. 5), using Binomial expansion we get,

$$Y_f(\alpha_s - \alpha_f)\Delta T whl = C\gamma_f nwd \quad (7)$$

$$d = \frac{Y_f(\alpha_s - \alpha_f)\Delta T hl}{Cn\gamma_f} \quad (8)$$

We know that the strain acting on the film is defined as,

$$\in = \frac{l}{L} = (\alpha_s - \alpha_f)\Delta T \quad (9)$$

Where l is the total change in length of the film, along the direction of the compressive stress and L is the total expanded length of the film after heating, along which the compressive stress starts acting when the system starts cooling down from the maximum temperature. Therefore,

$$l = L(\alpha_s - \alpha_f)\Delta T \quad (10)$$

This leads to our proposed Wavelength Equation,

$$d = \frac{Y_f[(\alpha_s - \alpha_f)\Delta T]^2 hL}{Cn\gamma_f} \quad (11)$$

Ascertaining the maximum length L of the film (i.e. the length of the film after heating) and the proportionality constant C directly isn't feasible. Therefore, (L/Cn) has been replaced by a proportionality constant C_w. It is a dimensional constant with units of length (i.e. meter when SI units are used for all other parameters). Thus, our final wavelength equation is,

$$d = C_w \frac{Y_f[(\alpha_s - \alpha_f)\Delta T]^2 h}{\gamma_f} \quad (12)$$

The proportionality constant C_w depends on the following parameters

i. More the **thermal expansion coefficient of the substrate** more is the tensile stress exerted by it on the film during heating. L is directly proportional to the tensile stress acting on the film. In case of PDMS, the thermal expansion coefficient varies with the curing temperature and also the duration of curing.

ii. More the **thermal expansion coefficient of the film** more is its expansion during heating, and more is the value of L. In case of thin films, the thermal expansion coefficient of a given material can also vary with the film thickness.

iii. Lower the **surface energy of a film,** the higher the surface area required to balance out a given stress. Thus, to balance out a given stress during heating, the expansion in length L will be more for a thin film material having lower surface energy. Thus, L is inversely proportional to surface energy.

iv. The higher the **tensile force acting on the film** while heating, higher is the expansion in it. Thus L is directly proportional to the tensile force acting on the thin film. The tensile force is dependent on the **Young's modulus** $(\boldsymbol{Y_f})$**, width** $(\boldsymbol{w})$**, and thickness of the film** $(\boldsymbol{h})$**, change in temperature of the system** $(\boldsymbol{\Delta T})$**, and the thermal expansion coefficient mismatch between the film and the substrate** $(\boldsymbol{\alpha_s - \alpha_f})$. (Refer SI equation 3).

v. L also depends on the initial length of the sample. Higher the initial length, higher is the expanded length L. However, it has been experimentally seen that beyond a critical length L_c, keeping other parameters constant, as L increases, n also increases such that the wrinkle periodicity doesn't change significantly. Below the critical length wrinkle formation does not take place.

2.3 Comparison of results from Wavelength Equation with experimental results

To model the above picture, we solve the Wavelength Equation for bilayer systems consisting of As_2Se_3 thin films deposited on PDMS substrates with arbitrary but reasonable choice of values for coefficients of thermal expansion for the substrate and film, and also for the surface energy and Young's modulus of the As_2Se_3 thin film. The selected values being $\alpha_{PDMS\,5} = 216 \times 10^{-6}/K$, $\alpha_{PDMS\,10} = 270 \times 10^{-6}/K$, $\gamma_{As_2Se_3} = 0.2 J/m^2$, $Y_{As_2Se_3} = 1 \times 10^{10} Pa$. The values lie within the respective ranges obtained from literature as enlisted in SI Section 1.2.

As shown in the following figures, for each trend in wrinkle wavelength periodicity as observed from the top view scanning electron microscope images, there exist parameters of Wavelength Equation which, when used to solve, give matching results.

2.3.1 Dependence of wrinkle wavelength on film thickness and temperature

Our Wavelength Equation predicts an increase in wrinkle wavelength with increase in film thickness and temperature.

Film thickness(nm)	Proportionality constant (C_w) with PDMS 5 substrate (m)
100	3.07×10^{-6}
150	3.11×10^{-6}
200	3.155×10^{-6}

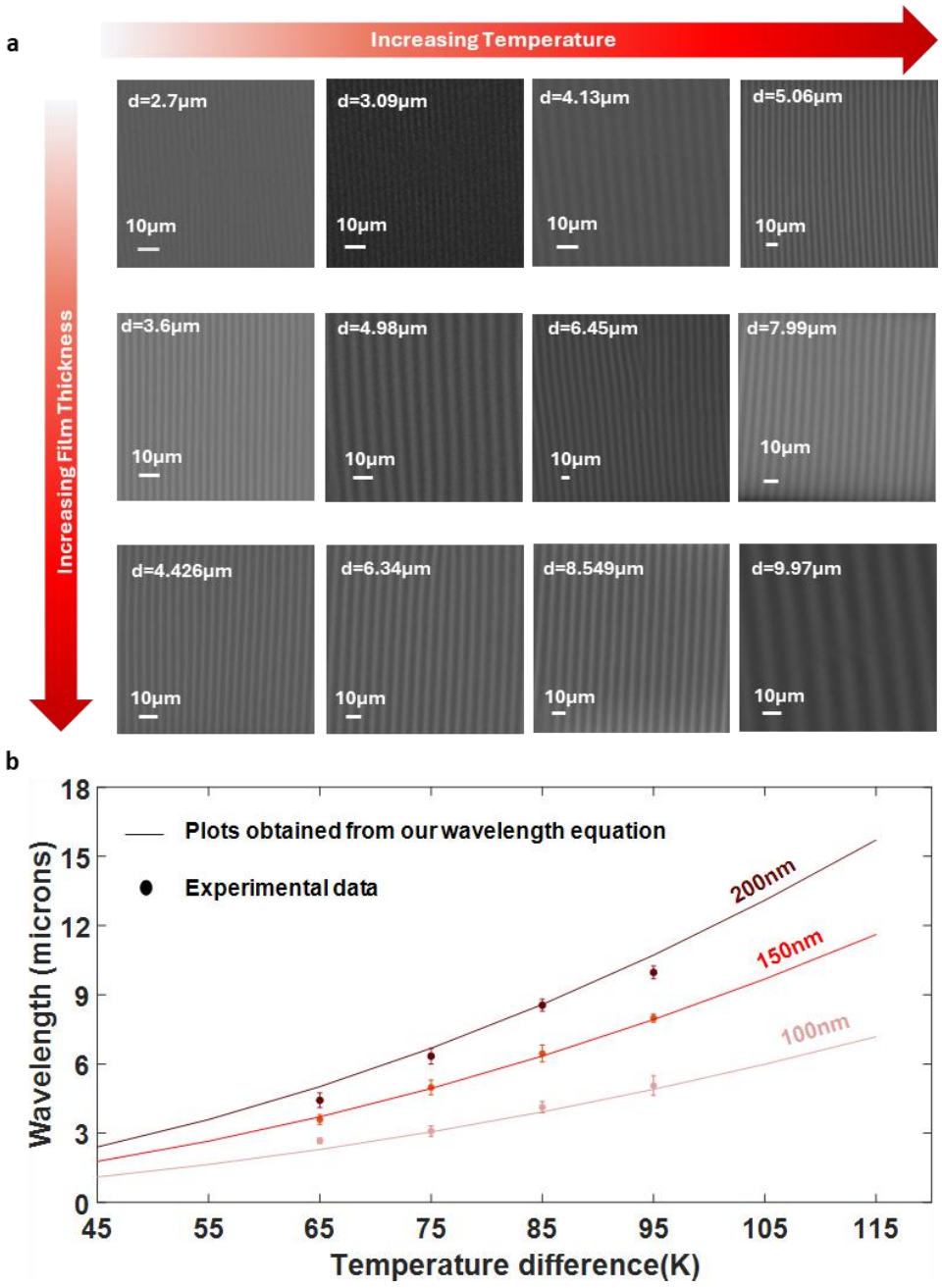

Figure 7| *(Top) Table showing the parameters used in the Wavelength Equation, for different film thicknesses, matching the modeling results with the experimental results. a, Comparison matrix of SEM images depicting the dependence of wrinkle wavelength on Film thickness and Heating Temperature. As the film thickness and heating temperature increases, the wavelength (d) also increases. Substrate: PDMS 5, Thin Film material: As_2Se_3. Heating temperature ranges from 90°C to 120°C, in intervals of 10°C and the room temperature is 25°C. The film thickness ranges from 100nm to 200nm in intervals of 50nm.*

According to our Wavelength Equation, an increase in film thickness and/or ΔT leads to an increase in the wavelength of the wrinkles. As the film thickness increases, the stress acting on it during the cooling process also increases, thereby increasing the wavelength (SI Equation 2). Similarly, as the heating temperature increases, the compression in the substrate while cooling down to room temperature also increases, thereby increasing the compressive stress on the film during the cooling process (SI Equation3).

SI Fig.7a depicts the dependence of wrinkle wavelength on film thickness and heating temperature. As the film thickness and heating temperature increases, the wavelength(d) also increases. The substrates are PDMS 5, with the thin film material being As_2Se_3. In SI Fig. 7a the heating temperature ranges from 90°C to 120°C, in intervals of 10°C and the room temperature (i.e. the cooling temperature) is 25°C. The film thickness ranges from 100nm to 200nm in intervals of 50nm. SI Fig. 7b illustrates the compatibility of our wavelength equation with the experimental results. The solid circles represent data from the experiments while the solid lines depict the corresponding plots obtained from the Wavelength Equation using similar parameters (i.e. thermal expansion coefficient of substrate and film, thickness, surface energy, Young's modulus of film and ΔT).

2.3.2 Dependence of wrinkle wavelength on thermal expansion coefficient mismatch between film and substrate

Our Wavelength equation predicts that as the difference in the thermal expansion coefficient between the film and the substrate increases, the wrinkle wavelength also increases.

As the difference in thermal expansion coefficients between the substrate and the rigid film deposited on it increases, so does the disparity in their thermal expansion. Consequently, as the system cools, the mismatch in contraction between the substrate and the film intensifies, leading to greater compressive stress on the film. This is why we observe larger wrinkles when there's a higher thermal expansion coefficient mismatch between the film and the substrate. PDMS10 has a higher thermal expansion coefficient than PDMS5, hence the wrinkles formed on the thin film deposited atop PDMS10 have higher wavelength than that deposited on PDMS5, for the same film material and film thickness (SI Fig.8). It is to be noted that mismatch between the theoretical and experimental values arises because all the thin film and substrate parameters have been assumed to be constant with respect to change in film thickness and system temperature. Also, in the theoretical model the sinusoidal wrinkles have been assumed to be triangular.

Film thickness(nm)	$C_w\ (m)$ with PDMS 5 as substrate	$C_w\ (m)$ with PDMS 10 as substrate
100	3.07×10^{-6}	3.15×10^{-6}
200	3.155×10^{-6}	3.2×10^{-6}

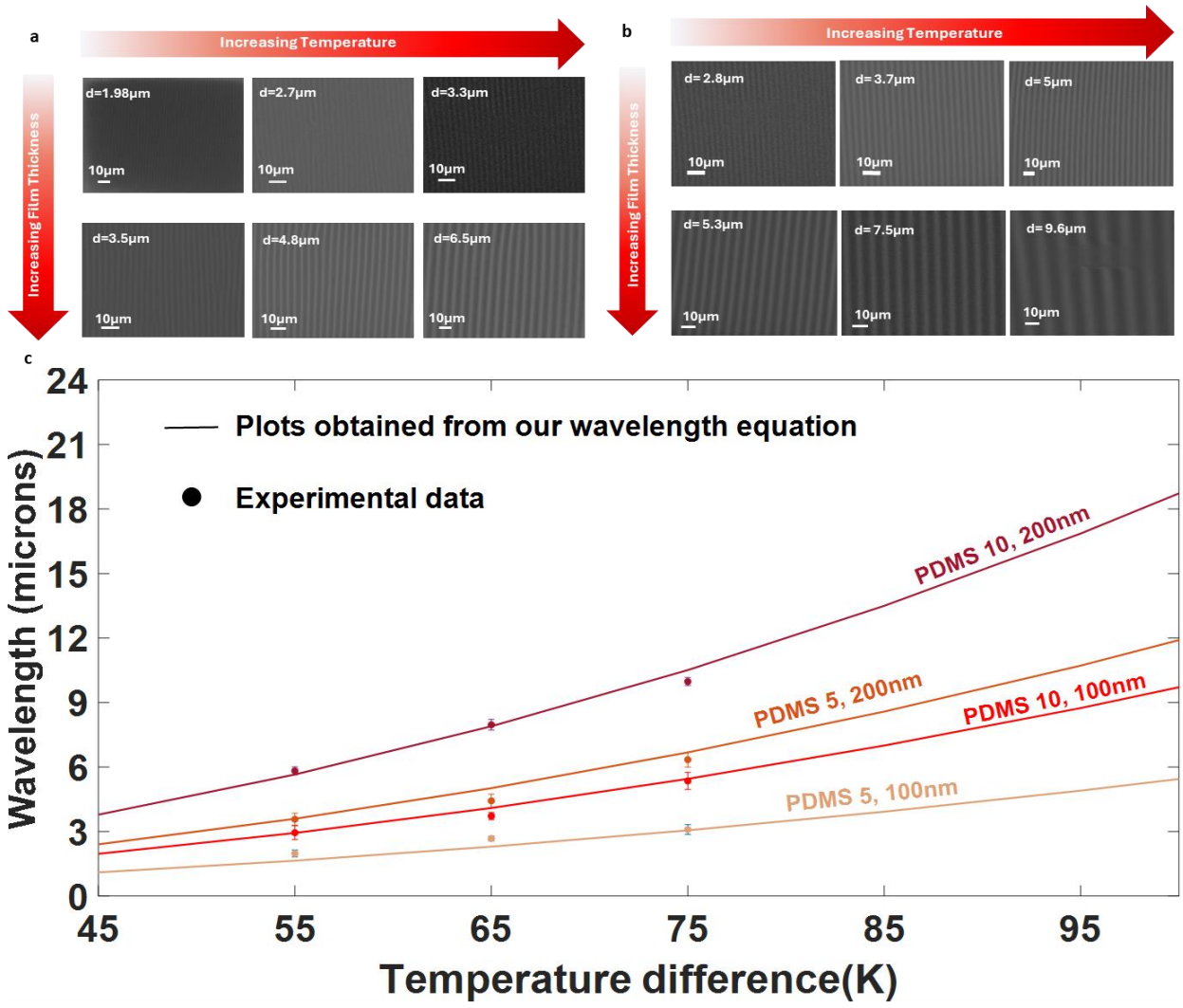

354

Figure 8| *(Top) Table showing the parameters used in the Wavelength Equation, for different film thicknesses for PDMS 5 and PDMS 10 substrates, matching the modeling results with the experimental results. a, Comparison matrix of SEM images with PDMS 5 as substrate. b, Comparison matrix of SEM images with PDMS 10 as substrate. (a-b), The temperature varies from* $80℃$ *to* $100℃$ *in intervals of* $10℃$ *. The film thickness are* $100\ nm$ *and* $200nm$*. Film material:* As_2Se_3 *c, Plot showing the dependence of wrinkle wavelength on the thermal expansion coefficient mismatch between the film and the substrate. The solid dots represent the experimental data points, and the solid lines are obtained from our Wavelength Equation using similar parameters.*

355

356 *2.3.2.1 Role of PDMS curing time on the thermal expansion coefficient mismatch between the*
357 *film and the substrate*

358 As the curing time of PDMS increases, the crosslinking between the PDMS base and the curing agent also
359 increases, thereby reducing its softness i.e. with increase in curing time the thermal expansion
360 coefficient of PDMS decreases

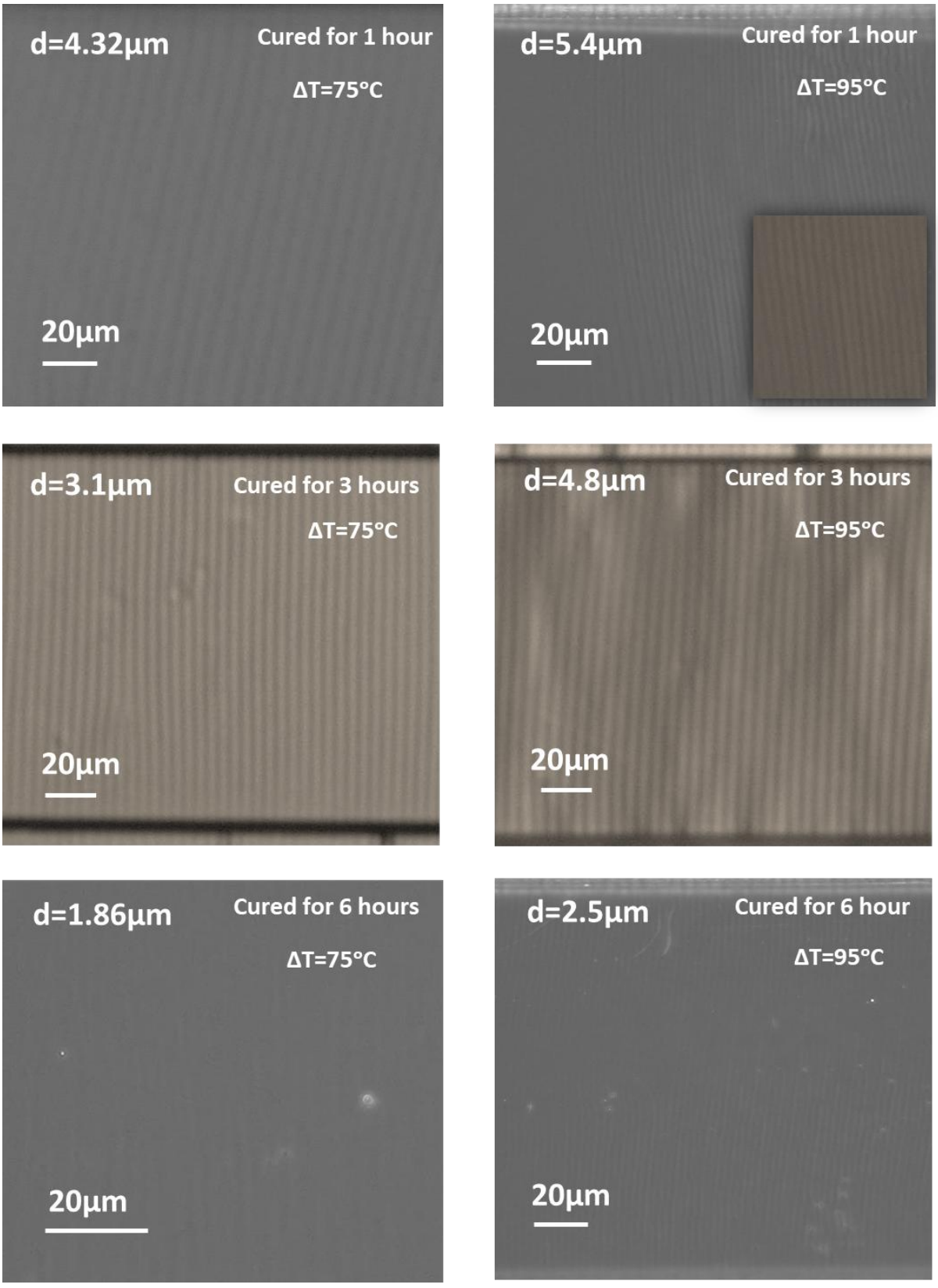

Figure 9| *This figure illustrates that, for the same film thickness, as the curing time of PDMS increases, the wavelength of the wrinkles formed in the bilayer system decreases. Substrate: PDMS 5, Thin film material:* As_2Se_3.

As the thermal expansion coefficient of the substrate decreases with increase in curing time, the mismatch in the thermal expansion coefficient between the film and the substrate also decreases, thereby reducing the stress acting on the film. Thus, by increasing the PDMS 5 curing time from 1 hour to 3 hours, the wavelength of wrinkles decreases from $4.32\mu m$ to $1.86\mu m$ for $\Delta T = 75$℃ and from $5.4\mu m$ to $2.5\mu m$ for $\Delta T = 95$℃. All the samples consist of 100nm As_2Se_3 deposited on PDMS 5 substrates.

When the compressive stress acting on the thin film in a single direction is high enough, non-linearities take place leading to paired wrinkles (SI Fig. 9 Top right). Such high stresses lead to high aspect ratio wrinkles (i.e. wrinkle amplitude being much higher than their wavelength), which merge at the wrinkle tips to form doubly paired wrinkles as illustrated in SI Fig. 9 Top right inset. Each doubly paired wrinkle has a very shallow indent at the top and acts as a single wrinkle.

2.3.3 Requirement of a critical film thickness for wrinkle formation

Compressive stress acting on a thin film is directly proportional to the thickness and Young's modulus of the film (Equation 3). Wrinkles manifest in a film when the stress energy due to a compressive force is balanced by the surface energy generated due to the formation of new surfaces. Consequently, a thin film with a higher surface energy will require a higher compressive stress for wrinkle formation. For instance, when being cooled down from 80℃ to 25℃, As_2Se_3, having a Young's modulus of $10^{10}Pa$, and surface energy of $0.2\ J/m^2$ requires a critical thickness exceeding 70nm for wrinkle formation, while materials like Ag and Al, boasting a Young's modulus of approximately $5 \times 10^{10}\ Pa$, and surface energy around $0.05 J/m^2$ exhibit a critical thickness of around 15 nm. Thus, we can see in SI Fig.10, wrinkles have formed in 15nm Ag and Al films but not on 60nm As_2Se_3 film

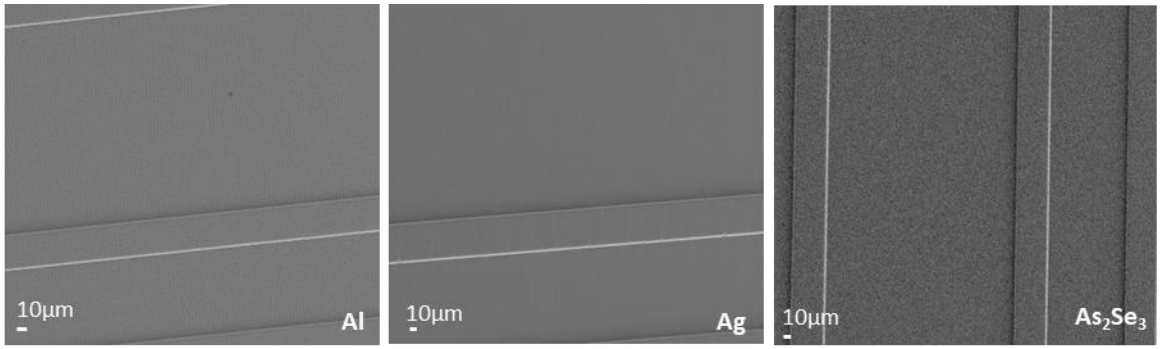

Figure 10|*SEM images showing wrinkle formation in 15nm Al and Ag thin films and the absence of wrinkles in 60nm As_2Se_3 thin films. All the thin films were deposited on PDMS5, heated to 80°C for 5 minutes and cooled down to 25°C.*

2.4 Prediction from the Wavelength Equation

Our wavelength equation can be efficiently used to find the thermal expansion coefficient of thin films by selecting appropriate values of the different parameters. (Refer Fig. 9 and Fig. 10).

Material	Film thickness(nm)	Surface energy (J/m^2)	Young's Modulus (Pa)	$\Delta T(K)$	Wavelength (μm)	$\alpha_s(K^{-1})$ PDMS 5	C_w ($\times 10^{-6}m$	$\alpha_f(K^{-1})$ (predicted from Wavelength Equation)	$\alpha_f(K^{-1})$ (reported in literature)
As_2Se_3	100	0.2	10^{10}	75	3.3	216×10^{-6}	3.07	22.3×10^{-6}	22×10^{-6}
Al	15	0.07	4.5×10^{10}	55	3.7	216×10^{-6}	3.5	25.51×10^{-6}	$18 - 30 \times 10^{-6}$
Ag	15	0.055	3.5×10^{10}	55	3.2	216×10^{-6}	3.15	27.57×10^{-6}	$19 - 31 \times 10^{-6}$

2.5 Requirement of a critical length for wrinkle formation and our proposed Critical Length Equation

By combining SI Equation 4 and SI Equation 10, the stress energy can be defined as

$$U = Y_f[(\alpha_s - \alpha_f)\Delta T]^2 whL \tag{13}$$

Thus, in order to overcome the critical stress required for wrinkle formation, the compressive stress should act along a length that is greater than the critical length required for the system. This is why as the distance between the grooves increases, the 1D wrinkles give way to 2D wrinkles because then both the lateral and longitudinal stress are greater than the critical stress required by that system for wrinkle formation (SI Fig. 11).

From SI Equation 7 and SI Equation 11 we can conclude that, if

$$L < C_l \frac{\gamma_f d}{Y_f h\left[(\alpha_s - \alpha_f)\Delta T\right]^2}$$

then wrinkle formation does not take place. Here C_l is a unitless proportionality constant and is $= Cn$. Thus, we arrive at the critical length equation which is defined as

$$L_c = C_l \frac{\gamma_f d}{Y_f h[(\alpha_s - \alpha_f)\Delta T]^2} \tag{14}$$

During the formation of 2D wrinkles the lateral and longitudinal stress are not equal. The lateral stress being lesser than the longitudinal stress, the periodicity of the wrinkles due to the lateral stress is lesser.

The proportionality constant C_l depends on the following parameters

i. For a given expanded length L, higher the compressive stress higher is the periodicity d and lower is the value of n. Since n is directly proportional to C_l, a decrease in the value of n also decreases C_l and the critical length L_c. Thus, for higher compressive stress the critical length decreases.

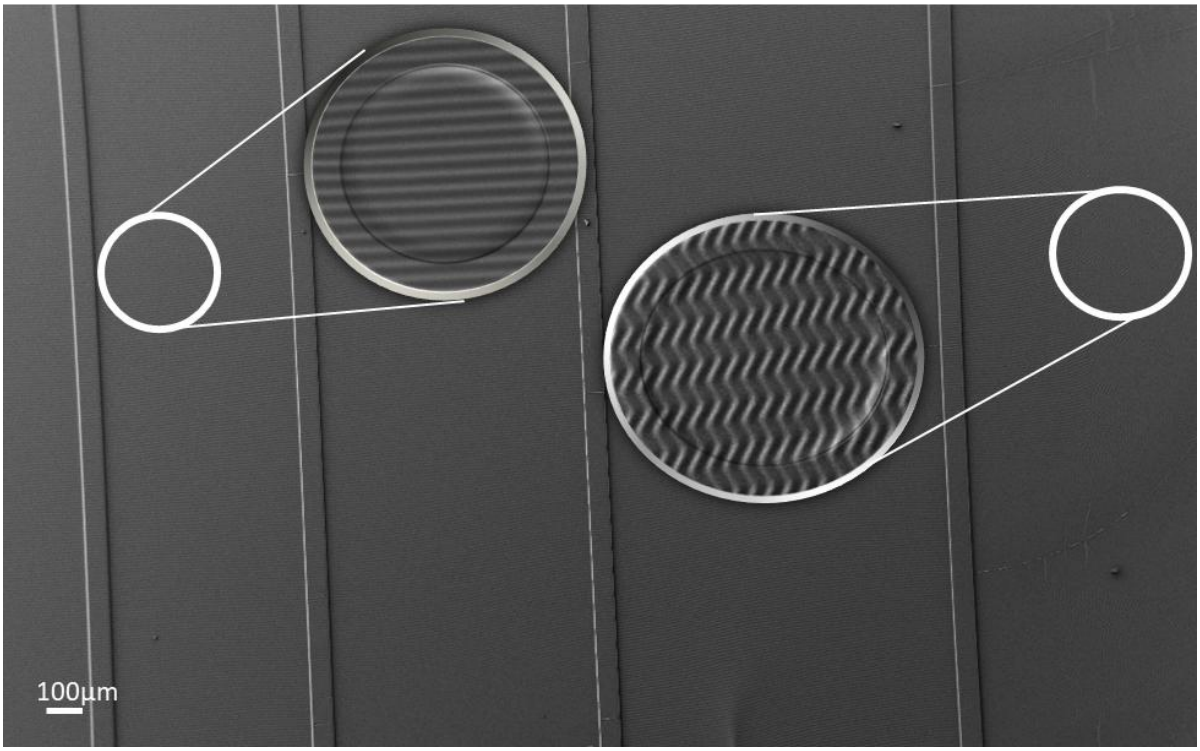

Figure 11|*Large area SEM image of wrinkled As_2Se_3 thin film on PDMS5 substrate. As the distance between the grooves increases to 1150µm, 2D wrinkles start appearing. Film thickness: 100nm, Heating temperature 120°C.*

2.6 Comparison of results from Critical Length Equation with experimental results

If any or all of ΔT, $(\alpha_s - \alpha_f)$ and h increases, then the stress acting on the film also increases, potentially allowing compressive stress along a shorter length to surpass the critical stress necessary for wrinkle formation. This explains why 1D wrinkles form when a 150nm As2Se3 film on PDMS5 is heated to 120°C and then cooled to 25°C, whereas 2D wrinkles emerge when the substrate is changed to PDMS10 while keeping other variables constant (SI Fig. 12a and b). This difference occurs because the thermal expansion coefficient of PDMS10 is higher than that of PDMS5.

Similarly, with increasing ΔT, L_c decreases. For instance, when a 150nm As_2Se_3 film deposited on PDMS10 is heated to 100°C, it forms 1D wrinkles, while 2D wrinkles appear at 120°C (SI Fig. 12b and c).

A reduction in the surface energy and an increase in the Young's modulus of the thin film material lowers the critical length. Consequently, 1D sinusoidal wrinkles are observed in a 100nm As_2Se_3 thin film (with $\gamma_f = 0.2 J/m^2$ and $Y_f = 1 \times 10^{10}\ Pa$) on a PDMS 5 substrate when heated to 80°C and subsequently cooled, whereas 2D wrinkles are observed in Ag and Al thin films, which have $\gamma_f \approx 0.04 J/m^2$ and $Y_f \approx 4 \times 10^{10}\ Pa$ under similar conditions (SI Fig. 12d, e and f). The critical Length equation has been experimentally found to be more accurate for well-ordered wrinkles, i.e. for wrinkles on As_2Se_3 thin films.

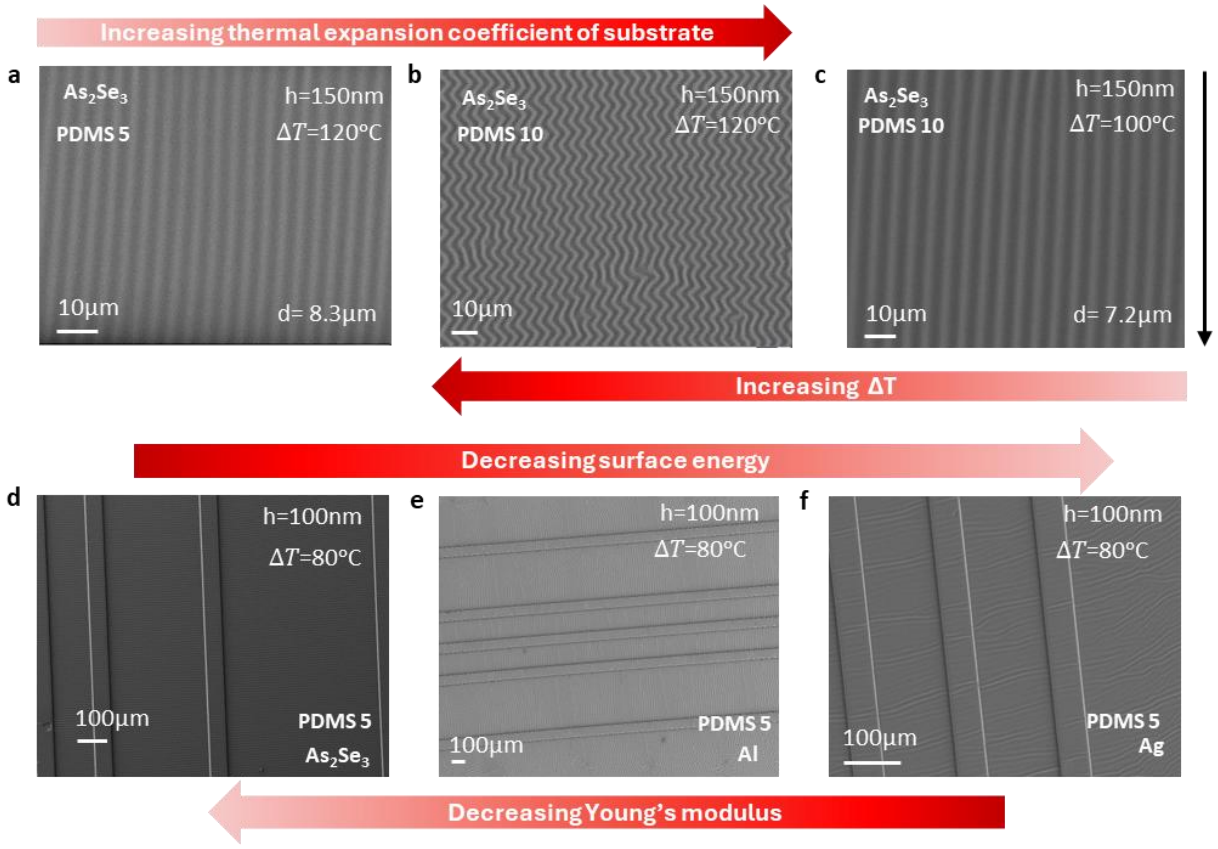

Figure 12|SEM images a, 150nm As_2Se_3 deposited on PDMS5, heated to 120°C. b, 150nm As_2Se_3 deposited on PDMS10, heated to 120°C. c, 150nm As_2Se_3 deposited on PDMS10, heated to 100°C. a-c, Lateral distance 950nm, black arrow indicates the direction of lateral distance. d, 100nm As_2Se_3 deposited on PDMS 5, heated to 80°C. e, 100nm Al deposited on PDMS 5, heated to 80°C. f, 100nm Ag deposited on PDMS 5, heated to 80°C. All the samples were cooled down to 25°C for wrinkle formation.

2D wrinkles or zigzag wrinkles are a superposition of two sets of 1D wrinkles formed along two different directions whereas, 3D wrinkles or labyrinth isotropic wrinkles are a superposition of multiple sets of 1D wrinkles formed along different directions.

2.6.1. Effect of heating temperature and substrate softness on wrinkle formation and critical length

As the heating temperature increases, the compressive stress acting on the thin film while it cools, also increases. Wrinkle formation requires the compressive stress acting on the thin film to be greater than its critical stress. The formation of large area, uniform, ordered wrinkles requires a uniform force acting on the film which can be achieved within an optimal temperature range. The lack of wrinkle formation at temperatures much below this range is attributed to the insufficient generation of compressive stress on the film (Figure 13). Conversely, when the system is heated to temperatures exceeding this range by a large extent, disorderedness starts in the thin films (Figure 14).

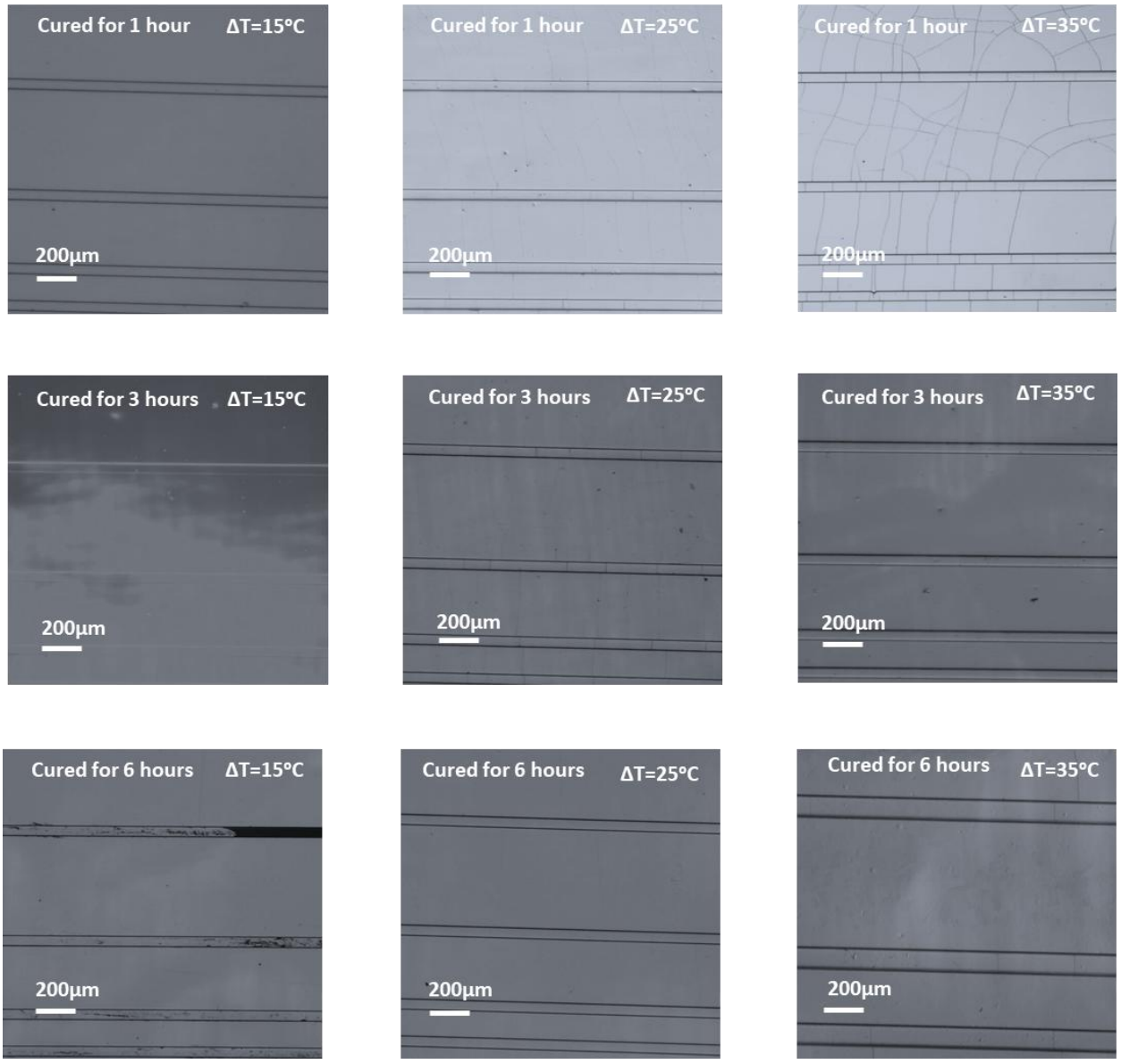

Figure 13| *Optical microscope images illustrating the absence of wrinkles in bilayer systems, consisting of 100nm As_2Se_3 thin films deposited on PDMS 5 substrates, when heated to temperatures lower than the optimum temperature range for the bilayer system. The PDMS substrates were cured for 1 hour (Top), 3 hours (Middle), and 6 hours (Bottom). The thermal expansion coefficient being higher in PDMS substrates cured for 1 hour, during heating the tensile stress acting over the film deposited atop is also higher leading to the formation of cracks as seen in the Top Right image. For substrates cured for 3 hours and 6 hours, cracks are absent.*

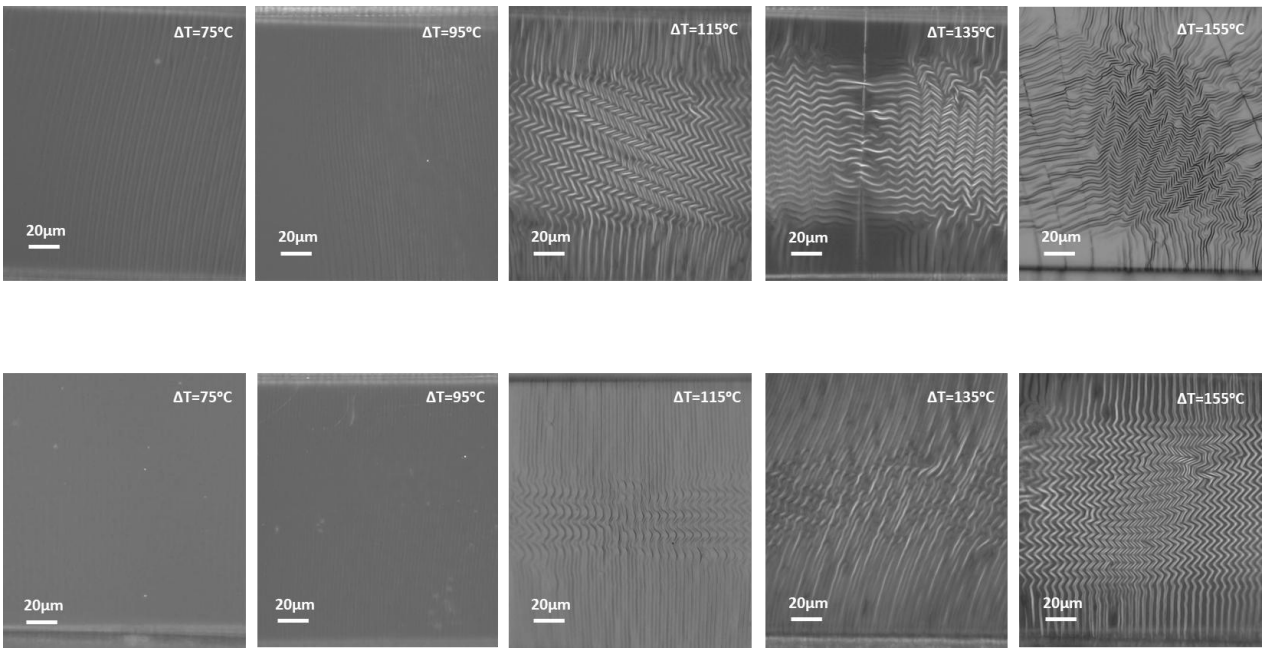

Figure 14| *Optical microscope images illustrating the effect of heating temperature on the orderliness of the wrinkles. Substrate: PDMS 5. Thin film material: 100nm As_2Se_3. (Top) Substrates cured for 1 hour. (Bottom) Substrates cured for 6 hours. As the heating temperature increases, the 1D ordered wrinkles give way to 2D wrinkles, finally leading to multiple cracks and disordered labyrinthine wrinkles. Again, the wrinkles are more ordered for substrates with higher curing time*

Figure 14 illustrates that as the heating temperature increases, 1D ordered wrinkles give way to 2D wrinkles, finally leading to multiple cracks and disordered labyrinthine wrinkles after cooling down to the room temperature $(25℃)$. As the curing time of the PDMS 5 substrate increases from 1 hour to 6 hours, the wrinkles become more ordered with respect to increase in heating temperature. For $\Delta T = 115℃$, 2D wrinkles have just started forming on PDMS substrates cured for 6 hours, whereas the 2D wrinkles are more prominent on substrates cured for 1 hour. At $\Delta T = 135℃$, cracks have started forming for substrates cured for 1 hour. At $\Delta T = 155℃$, multiple cracks have formed leading to disordered labyrinthine wrinkles on the substrates cured for 1 hour, whereas the substrate cured for 6 hours still has 2D wrinkles, with much lesser number of cracks. Thus, the critical length decreases with increase in heating temperature and duration of curing of PDMS substrate.

3. PHYSICS OF WRINKLED SURFACES ACTING AS DIFFRACTION GRATINGS

3.1 Origin of diffraction spots from an ordered sinusoidal surface

Diffraction occurs when a wave encounters an obstacle or aperture that causes it to bend around corners or spread out thereby producing periodic alterations in its phase, amplitude or both. The origin of diffraction spots from an ordered sinusoidal surface can be understood through Huygens-Fresnel principle and wave interference. According to this principle, every point on a wavefront can be considered as a source of secondary spherical wavelets. When a wavefront encounters an obstacle, these secondary wavelets interfere with each other constructively and destructively, leading to the formation of a diffraction pattern. An ordered sinusoidal surface acts as a reflection-based diffraction grating because its crests resemble a repetitive array of diffracting elements i.e. obstacles for an incoming wave of light. Each part of the surface acts as a source of secondary wavelets, and the interference between these wavelets results in constructive interference in certain directions and destructive interference in others. The diffraction orders and the spacing between the spots depend on the periodicity of the wrinkles (which is equivalent to the periodicity of the wrinkle crests), the angle of incidence, wavelength of the incident wave and the angle of detection.

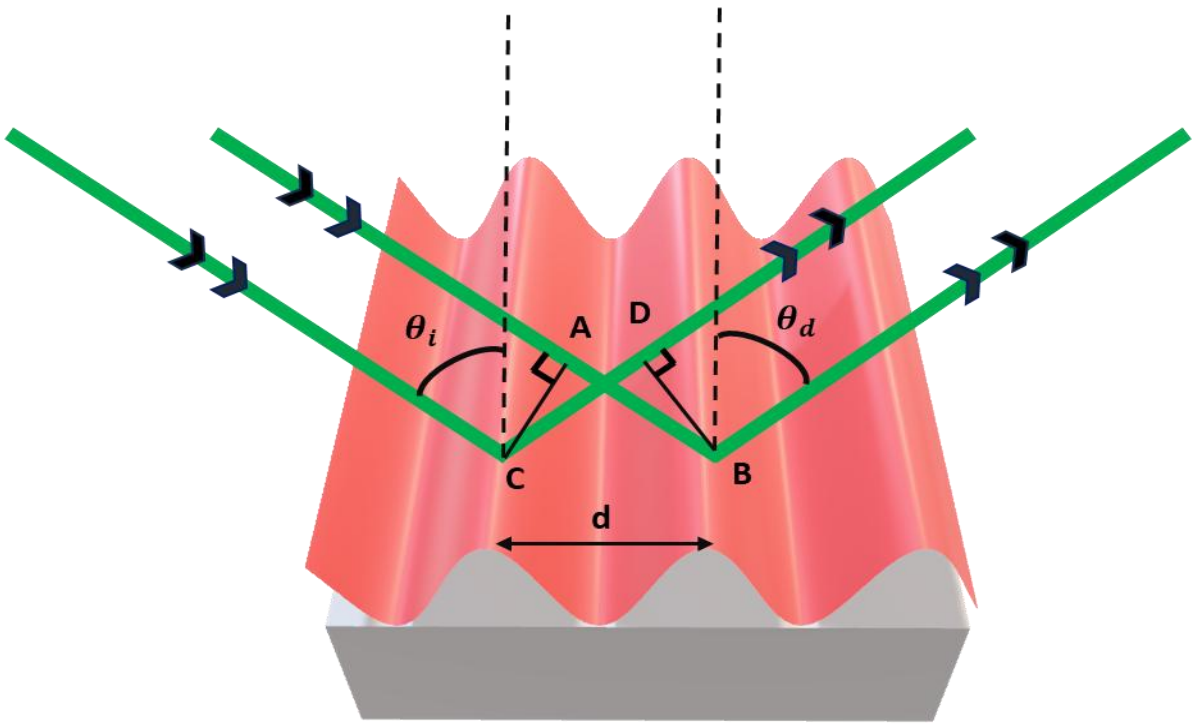

Figure 15|*Schematic of diffraction from a wrinkled surface of periodicity d. Angle of incidence is* θ_i *, angle of detection of rays is* θ_d*. If the wavelength of the waves is λ, for constructive interference the path difference between two adjacent waves should be an integral multiple of λ, i.e.* $CD - AB = m\,\lambda$*, where m is an integer.*

When plane waves of wavelength λ are incident at an angle θ_i, on a wrinkled surface of periodicity d, in order to get constructive interference at a detection angle θ_d , the following relation must be satisfied

$$CD - AB = m\lambda$$

Where m is an integer and also the diffraction order. Therefore, we get the relation,

$$d \sin\theta_d + d \sin\theta_i = m\lambda$$

$$m\lambda = d(\sin\theta_d + \sin\theta_i) \quad (15)$$

Thus, for a given wavelength (λ) of incident light, incident at an angle θ_i , we can get different diffraction orders by tuning the periodicity of the wrinkles.

3.2 Orientation of diffraction spots

The alignment of the diffraction spots relies on the orientation of the plane of incidence relative to the direction of the wrinkles. When the plane of incidence is oriented parallel to the direction of the wrinkle array, vertical diffraction spots appear. Conversely, if the plane of incidence is perpendicular to the wrinkle array's direction, horizontal diffraction spots are observed.

As we know that the diffraction spots represent the hkl planes in the reciprocal lattice of the Bravais lattice, the ordered wrinkles are analogous to a set of parallel hkl planes. As the orientation of the wrinkles with respect to the incident plane changes, the hkl plane also changes thereby altering the orientation of the diffraction spots. This is why we get circular diffraction patterns for isotropic labyrinth wrinkles. These ring like diffraction patterns find applications in cataract surgeries where circular incisions are needed to be made.

In SI Fig. 16 we can see that as the orientation of the wrinkles with respect to the incident beam plane changes from 0° to 90° in steps of 30°s, the orientation of the diffraction spots also changes.

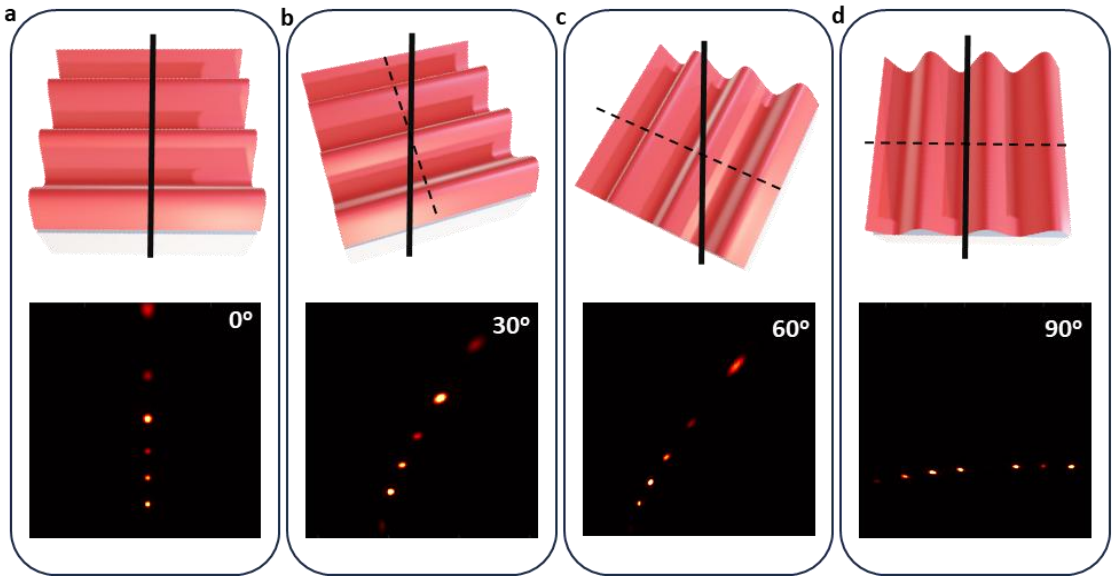

Figure 16| *Schematics depicting the orientation of wrinkles and the corresponding simulation images for the diffraction spots. The simulations were done for a periodicity of 6.2μm, amplitude of 400nm and incident light of wavelength 500nm.*

3.3 Wrinkles for optical diffusion

Disordered labyrinthine wrinkles can be considered as superposition of multiple sets of 1D sinusoidal wrinkles at different angles to each other. Thus, when light diffracts over disordered labyrinthine wrinkles, ring like circular diffraction patterns are formed on the detector screen. These wrinkles form when the samples are heated to sufficiently high temperatures followed by subsequent cooling. During cooling as the temperature of the bilayer system decreases, the wavelength and the disorderliness of the wrinkles increases. This subsequent cooling leads to an increase in the number of diffraction rings formed on the screen

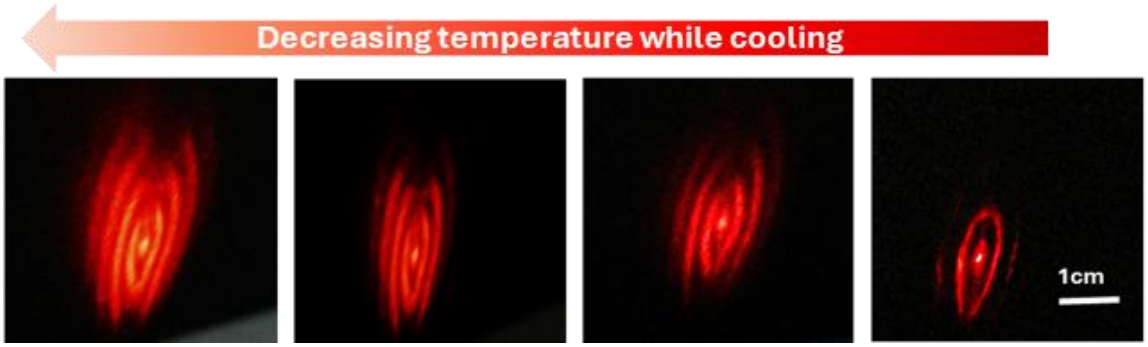

Figure 17| *Experimental images of a tunable optical diffuser, illustrating the dependency of diffraction rings on the cooling temperature*

3.4 Disappearance and reappearance of colors during thermal processing

When the wrinkled samples are heated to sufficient temperature the wrinkles disappear due to the thermal expansion in the thin film and also due to the tensile stress acting on it because of the thermal expansion mismatch between the film and the substrate. Diffraction doesn't take place in the absence of wrinkles i.e. on a flat surface, thereby leading to the disappearance of colors on being heated. On subsequent cooling the colors reappear due to the formation of wrinkles which diffract light. The samples are responsive to simple thermal heating as well as joule heating (since both lead to an increase in temperature of the bilayer system), thereby making them excellent candidates for adaptive visible camouflage

3.5 Dependence of diffraction orders on temperature

As discussed before, as the heating temperature increases the wavelength(periodicity) of the wrinkles also increases, thereby increasing the number of diffraction orders. For a given wavelength and angle of incidence of incident light, more the periodicity, the more the diffraction orders observed (SI Equation 15).

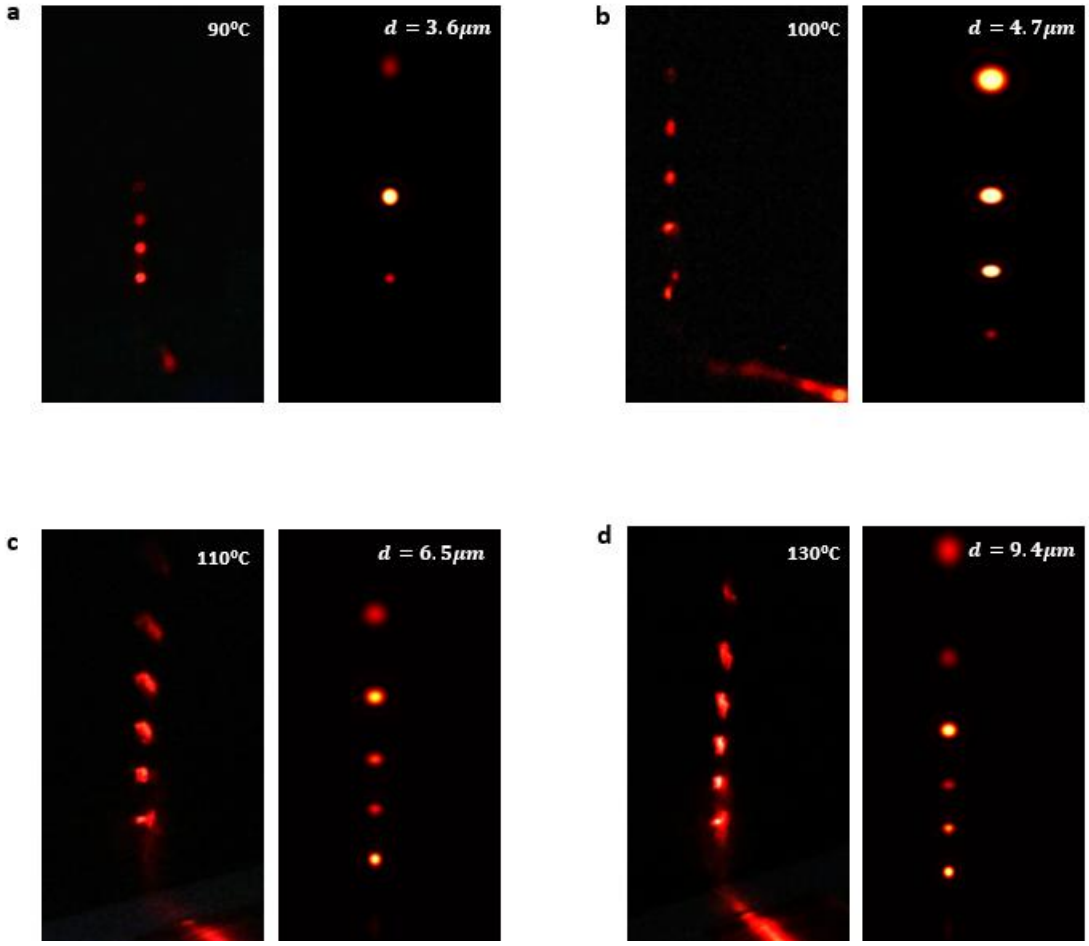

Figure 18| *Experimental images(left) and corresponding simulation images(right). Sample: 150nm As_2Se_3 deposited on PDMS 5. a, heated to 90°C to get wavelength of 3.6μm. b, heated to 100°C to get wavelength of 4.7μm. c, heated to 110°C to get wavelength of 6.5μm. d, heated to 130°C to get wavelength of 9.4μm.*

In SI Fig. 18, the experimental images(left) and the corresponding simulation images (right) illustrate how the number of diffraction orders increases due to the increase in periodicity of the wrinkles when the same sample is heated to different temperatures followed by subsequent cooling.

3.6 Simulation of diffraction spots

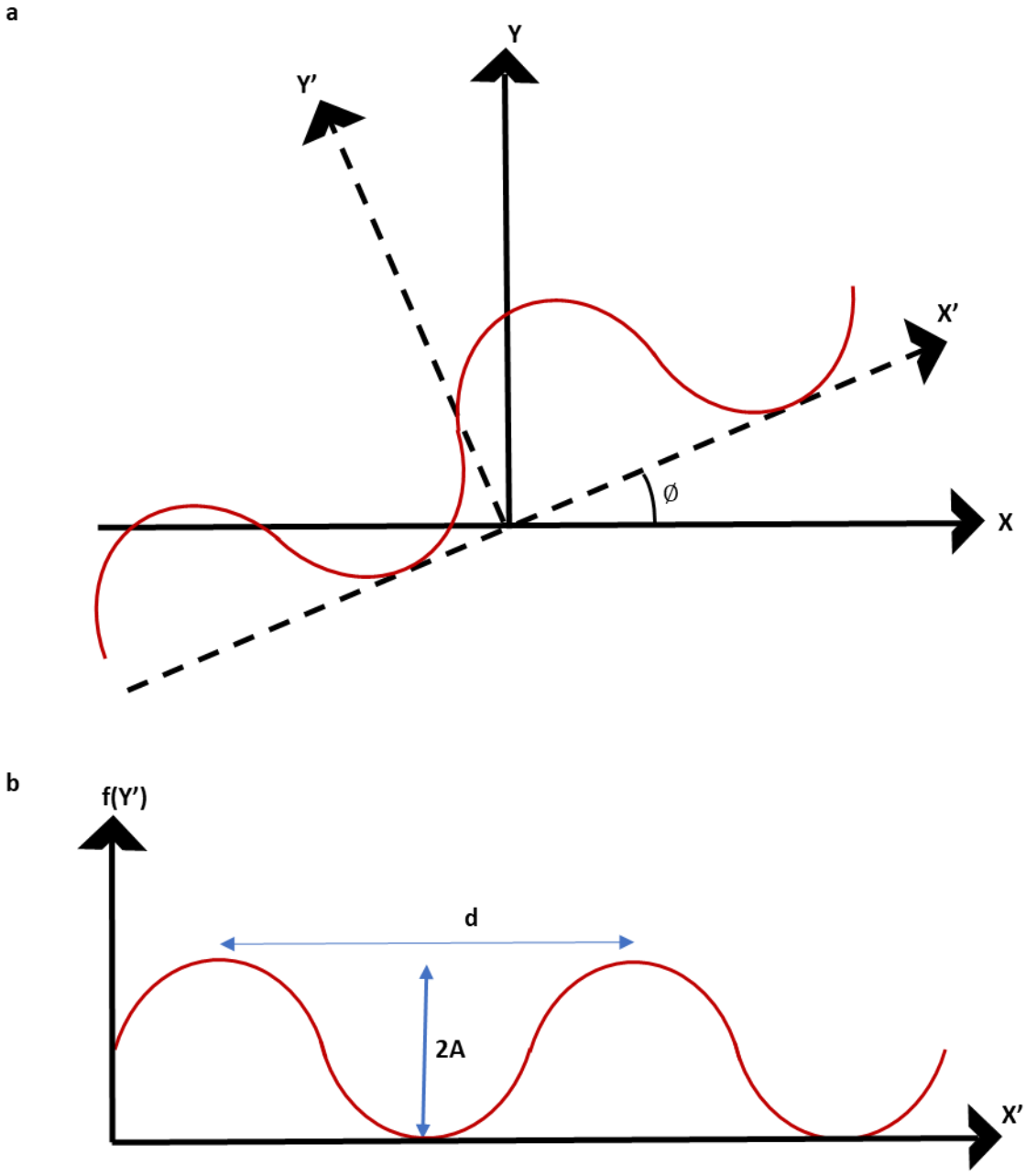

Figure 19| *a, A global coordinate system (X, Y), a local coordinate system (X',Y') rotated by an angle Ø with respect to global coordinates and a sinusoidal variation along X' axis. b, Cross-sectional image of the sinusoidally varying function along X' axis.*

For the MATLAB simulations we have considered two coordinate systems, a global coordinate system (X, Y) and a local coordinate system (X', Y') rotated by an angle Ø with respect to the global coordinates and have placed a sinusoidally varying function along the X' axis, as shown in SI Fig.19a. The cross-sectional image shown in SI Fig.19b illustrates that the function of the sinusoidal structure can be defined as,

$$f = A + Asin(k_d X')$$

Where $k_d = 2\pi/d$ and d is the periodicity of the structure. For normal incidence of light along -Y direction, since the amplitude of the structure is very low as compared to its periodicity, the phase profile on the (X', Y', 2A) plane can be defined as,

$$\emptyset(X', Y') = k_0(2l(X')) \tag{17}$$

Where $l(X') = 2A - f$

Therefore,
$$l(X') = A - Asin(k_d X') \tag{18}$$

The local co-ordinates is related to the global co-ordinates by the rotation matrix and the relation is defined as,

$$\begin{pmatrix} X' \\ Y' \end{pmatrix} = \begin{pmatrix} cos\emptyset & sin\emptyset \\ -sin\emptyset & cos\emptyset \end{pmatrix} \begin{pmatrix} X \\ Y \end{pmatrix} \tag{19}$$

From this relation we get,

$$X' = Xcos\emptyset + Ysin\emptyset \tag{20}$$

Thus,
$$l(X, Y) = A - Asin(k_d(Xcos\emptyset + Ysin\emptyset)) \tag{21}$$

and the phase is defined as

$$\emptyset(X', Y') = k_0 2(A - Asin(k_d(Xcos\emptyset + Ysin\emptyset))) \tag{22}$$

Ignoring the constant phase we get,

$$\emptyset_1(X', Y') = -k_0 2Asin(k_d(Xcos\emptyset + Ysin\emptyset)) \tag{23}$$

Considering the light to be incident along X axis, making an angle θ with respect to Y axis, the additional phase due to this angle of incidence is defined as,

$$\emptyset_2(X, Y) = k_0 Xsin\theta \tag{24}$$

Therefore, the net phase in the plane (X', Y', 2A) is defined as,

$$\emptyset(X, Y) = \emptyset_1(X, Y) + \emptyset_2(X, Y) \tag{25}$$

And the corresponding filed is,

$$E(X, Y) = e^{i[k_0 xsin\theta - 2k_0 Asin(k_d(Xcos\emptyset + ysin\emptyset))]} \tag{26}$$

Considering a finite size of the aperture i.e. limiting the spot size, the field is defined as,

$$E(X, Y) = \begin{cases} e^{i[k_0 xsin\theta - 2k_0 Asin(k_d(Xcos\emptyset + ysin\emptyset))]}, & \sqrt{(X^2 + Y^2)} \le R \\ 0, & \sqrt{(X^2 + Y^2)} > R \end{cases} \tag{27}$$

Where R is the radius of the spot.

We have ignored the edge effects since we are in scalar diffraction theory regime as R is very large compared to the periodicity of the sinusoidal structure. Once the field on the Z=2A plane is known, we can calculate the field at any point (x_0,y_0,z_0) using the Ray Sommerfeld diffraction formula which is defined as,

$$E(x_0, y_0, z_0) = \iint_{-\infty}^{\infty} \frac{E(X,Y,Z)}{\lambda} \left(\frac{1}{kl_0} - i\right) \frac{(Z-2A)}{l_0} \frac{e^{ikl_0}}{l_0} dxdy \quad (28)$$

Where $l_0 = \sqrt{(2-2A)^2 + (X-x_0)^2 + (Y-y_0)^2}$ and λ is the wavelength of the incident monochromatic light. Using SI Equation 28 we calculate the field at a plane Z=1cm (since in our experiments the plane was placed at a distance of 1cm from the sample) to get the diffraction patterns.

4. ROLE OF WRINKLES IN INCREASING THE OUT-COUPLING EFFICIENCY

We know that when a ray passes from a medium of higher refractive index to lower refractive index, if the angle of incidence is higher than the critical angle for that pair of media, then total internal reflection (TIR) takes place. TIR reduces the outcoupling efficiency of encapsulated light sources and photovoltaics like solar cells. The presence of wrinkles in the top-most layer increases the critical angle for a pair of media thereby increasing the out-coupling efficiency. This happens because of the change in the position and angle of the normal to the free surface of a film, as illustrated in SI Fig. 20a and b. When an LED is encapsulated by a wrinkled surface consisting of transparent PMMA wrinkles on PDMS substrate, the detector registers a power of 3.526mW, whereas when it is encapsulated by plain PDMS, the detector detects a power of 2.779mW (Figure 6b). Figure 6c shows the simulation result for the above experiment. Wrinkled surface shows a transmittance of 98% as compared to a transmittance of around 87% when encapsulated by an unpatterned PDMS substrate (depicted in SI Fig. 21)

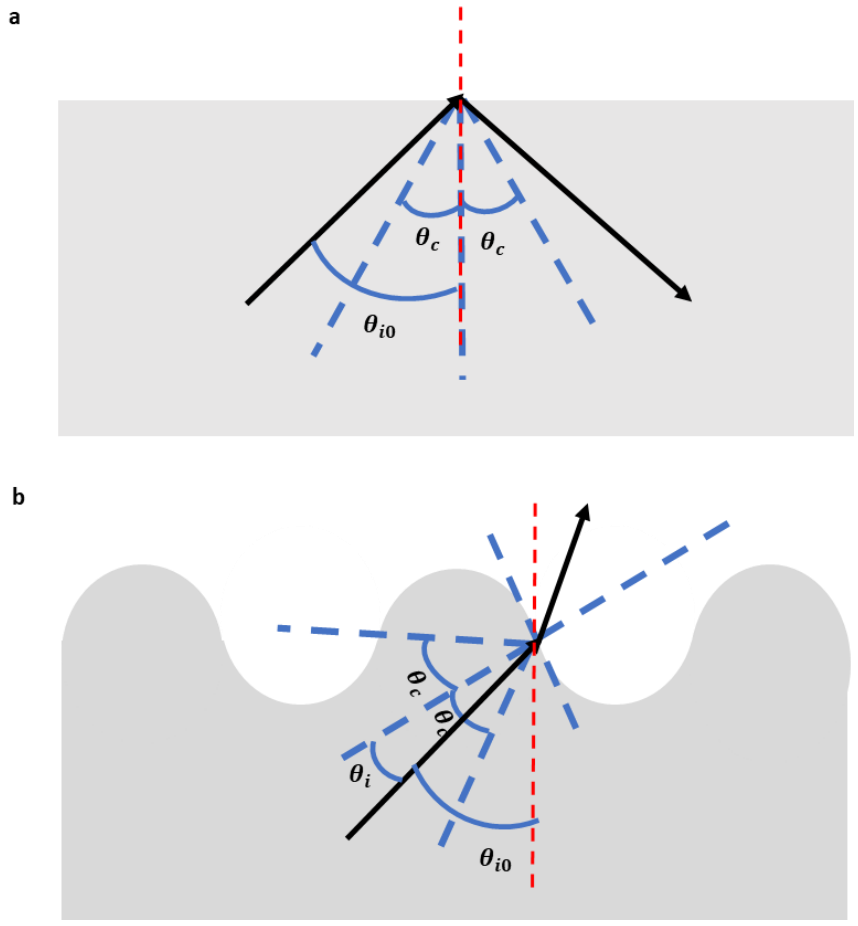

Figure 20| *a, schematic showing TIR when the angle of incidence of a beam going from a higher refractive index to lower refractive index is greater than the critical angle of a given pair of media, i.e.* $\theta_{i0} > \theta_c$*. b, schematic showing the absence of TIR even when the angle of incidence of a beam going from a higher refractive index to lower refractive index is greater than the critical angle (with respect to the normal to the plane surface) of a given pair of media, i.e.* $\theta_i < \theta_c$ *even though* θ_{i0} *is still the same.*

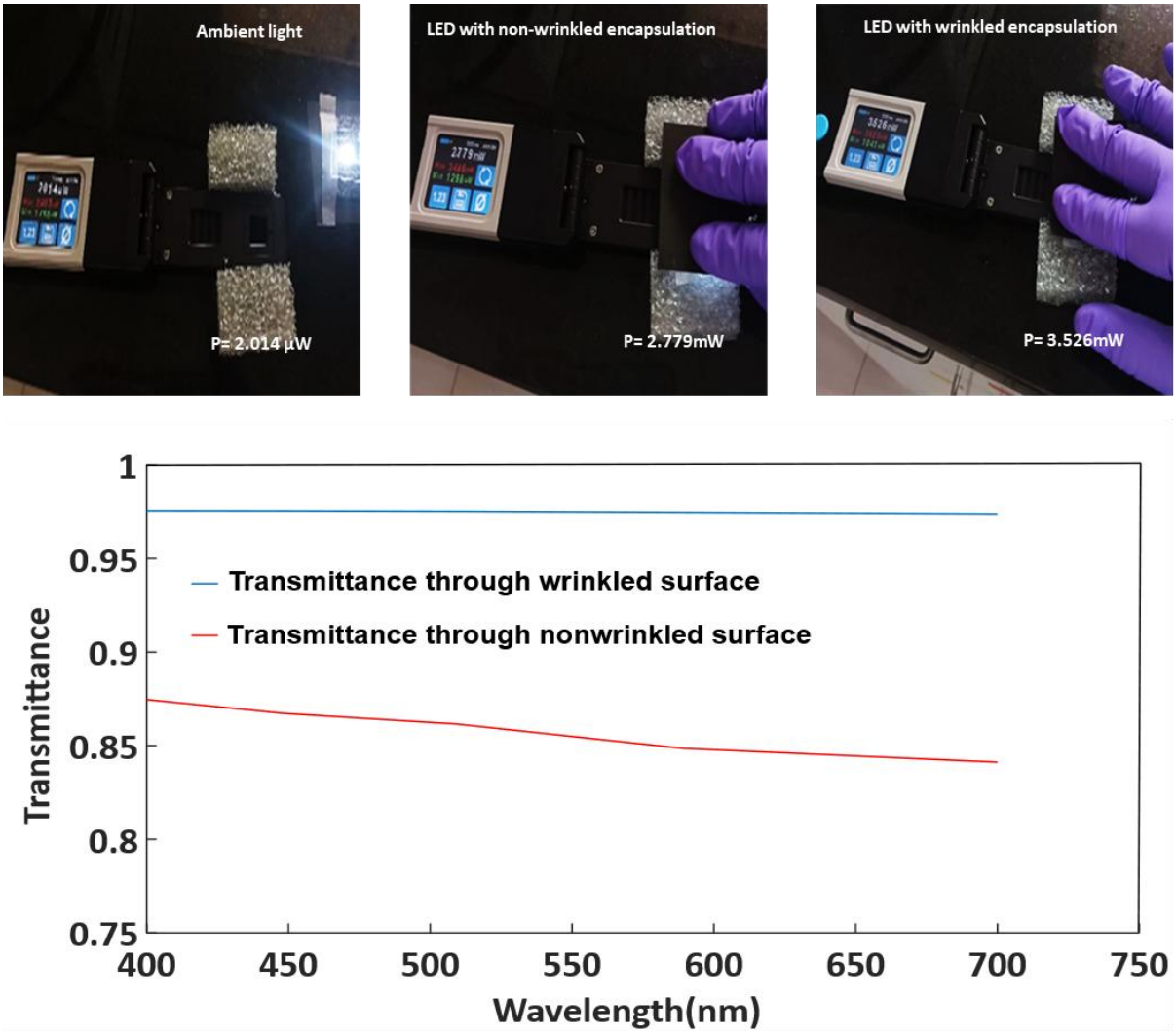

Figure 21| *a, Increase in out-coupling efficiency of encapsulated light sources. LED lights encapsulated by transparent wrinkles (PMMA wrinkles on PDMS substrate) register higher power as compared to those encapsulated by flat unpatterned PDMS. When the LED is encapsulated by a wrinkled surface, the detector registers a power of 3.526mW, whereas when it is encapsulated by plain PDMS, the detector detects a power of 2.779mW. b, shows the simulation result for the above experiment. The wrinkled surface shows a transmittance of 98% as compared to a transmittance of around 87% when encapsulated by an unpatterned substrate.*

5. NOVELTY OF THE WORK

5.1 Novelty in the processing (Ordered, Large area, Defect-free), Calibration, Materials and Applications

While wrinkles have been fabricated through various techniques, such as LASER treatment, exposure to UV, visible, or NIR light, plasma treatment, chemical swelling, mechanical strain induction, and thermal annealing, most of them suffer from limitations such as restricted fabrication area, the presence of defects like cracks and delaminations, and disorderliness. Here, we utilize a straightforward thermal processing approach to achieve large area, orderly, and defect-free wrinkles. In this work, we demonstrate, for the first time, a simple calibrated method for the formation of wrinkles of desired periodicity and orientation. Additionally, we have explored various thin film materials like chalcogenides, metals, and polymers, confirming the versatility of our method across these materials.

Attached is a table highlighting the novelty of our work in comparison to existing similar studies.

Sl No.	Thin film processing technique	Substrate	Thin film material	Defects formed	Calibrated with respect to structure causing stimuli	Type of structures formed	Applications	Reference
1	**Electrically** Suitable voltage bias and its reverse applied to a thin film stack of amorphous iron oxide and silver to float the silver layer above or below the oxide layer by the migration of silver atoms	Si wafers with $1\mu m$ thermal oxidized layer and polyethylene terephthalate	Stacked multilayer of TiW/Ag/Fe_2O_3 /ITO	Disorderedness in the atomic arrangement of amorphous Fe_2O_3 affects the quality of the devices	No	Floating thin film layer	Dynamic structural color	[14]
2	**Mechanically** Uniaxial stretching of the PDMS/thin film system	PDMS	PVA/Laponite composite	No	No	Disordered cracks	Mechanochromic devices with capabilities like changing transparency, switching luminescence	[15]
3	**Mechanically** Formation of thin layer of SiO_x on UVO treated PDMS, Uniaxial stretching of PDMS substrate, Poisson effect causing compressive stress and leading to wrinkle formation in direction perpendicular to the stretching direction	PDMS	-	Cracks	Yes (wrinkle periodicity as a function of pre-strain)	disordered sinusoidal wrinkles	Tunable optical transmittance, Smart windows, Switchable elastomeric display	[16]

Sl No.	Thin film processing technique	Substrate	Thin film material	Defects formed	Calibrated with respect to structure causing stimuli	Type of structures formed	Applications	Reference
4	**Mechanically** Carbon nanotube solution spray-coated on PDMS substrates followed by uniaxial and biaxial mechanical stretching to alter the morphology of the nanotubes	PDMS	Carbon nanotube solution	Not reported	No	Isotropic orientation of buckled nanotubes	Pressure and strain sensors	[17]
5	**Mechanically** Spin-coating of polymer films on UV treated Si wafer and placing cured PDMS films on the supported polymer films, Transferring the polymer films onto PDMS substrates by immersing the system in water, Wrinkle formation upon applying mechanical strain on the film/PDMS system	PDMS	PS	Cracks	No	1D ordered sinusoidal wrinkles	Measuring elastic moduli of thin polymer films	[18]
6	**Mechanically** Spin-coating of LC polymer films on UV treated Si wafer and placing cured PDMS films on the supported polymer films, Transferring the polymer films onto PDMS substrates by immersing the system in water at room temperature for 10 hours, Achieving wrinkle formation through lateral uniaxial compression on the polymer/PDMS system using a Hoffman type pinchcock	PDMS	Az containing LC polymer	Not reported	No	Partially ordered 1D sinusoidal wrinkles	Not shown	[19]

Sl No.	Thin film processing technique	Substrate	Thin film material	Defects formed	Calibrated with respect to structure causing stimuli	Type of structures formed	Applications	Reference
7	**Mechanically+ Thermally** Biaxial pre-stretching of air plasma treated and silanized PS substrates, Incubation in APTES solution to form molecular linking layer on the substrate, Pattern-masking and incubating in Au nanoparticle solution to form Au seed layer, Depositing continuous Au film through electroless deposition on seed layer, Formation of wrinkles on thin film through thermal processing	PS	Au	Not reported	No	Disordered isotropic folds	SERs based substrates	[20]
8	**Mechanically** Spin-coating PS or PS/Plasticizer films onto polished hydrophilic Si wafers. Transferring the polymer films onto PDMS substrates by immersing in water, Achieving wrinkles by applying uniaxial compressive strain	PDMS	PS	Not reported	No	Ordered sinusoidal wrinkles	Measurement of residual stress in polymer films	[21]
9	**Mechanically** Spin-coating PU and TiO_2 sol on PDMS substrates followed by heat treatment and oxygen plasma treatment. Achieving wrinkles by applying mechanical strain on the system	PDMS	PU and TiO_2 sol	Not reported	No	Partially ordered 1D wrinkles	Anti-counterfeiting photonic patterns	[22]
10	**Mechanically +Chemical Swelling** (i) Sequential stretching of oxygen plasma treated PDMS substrate leading to wrinkle formation (ii) DI water swelling of PHEMA films deposited on UV exposed rigid substrates leading to wrinkle formation	PDMS	Composite of PHEMA+ EGDMA	Not reported	Method (i) is calibrated d(λ) as a function of critical strain	1D and 2D ordered wrinkles, isotropic disordered wrinkles and creases	Tunable wetting and adhesion, tunable open channel micro-fluidics, strain responsive micro-lens arrays	[23]

676

677

Sl No.	Thin film processing technique	Substrate	Thin film material	Defects formed	Calibrated with respect to structure causing stimuli	Type of structures formed	Applications	Reference
11	**Chemical Swelling** Coating and curing liquid PDMS on PVA films deposited on rigid foundations, Peeling off the PVA/PDMS from the liquid foundation, Preparing 3 types of wrinkles by proper exposure to UV, oxygen and moisture	PDMS	PVA	Not reported	No	Isotropic labyrinthine wrinkles	Anti-counterfeit tags, Smart displays, Water indicators, Light diffusers, Antiglare films	[24]
12	**Chemical Swelling** Controllable swelling of sugar particles infused polymer matrices immersed in water, Deposition of conducting thin films on swollen substrates to obtain wrinkled thin films upon shrinking.	PDMS, Ecoflex	Au, Graphene	Not reported	No	Isotropic labyrinthine wrinkles	Soft electronics	[25]
13	**Chemical Swelling** UVO treatment of PS solution spin-coated on Si wafer, Swelling induced surface wrinkling by exposure of PS film to toluene vapours	Si	PS	Not reported	No	Isotropic circular wrinkles, Spokes, Targets, Labyrinths, Dots	Not shown	[26]
14	**Chemical Swelling** Peeling off cured PDMS stamp from structured Si master, Immersing the PDMS substrates in Aniline solution of required monomer concentration and polymerization at 2-5°C for 20 minutes to form PANI films, Wrinkled and dewrinkled states achieved in PANI film through swelling/deswelling via acid doping and base dedoping	PDMS	PANI	Multiple repetitions of doping/ dedoping causes cracks and delaminations	No	Isotropic labyrinthine wrinkles, Ordered 1D sinusoidal wrinkle strips of width 1-10μm	Smart display	[27]

678

679

680

681

Sl No.	Thin film processing technique	Substrate	Thin film material	Defects formed	Calibrated with respect to structure causing stimuli	Type of structures formed	Applications	Reference
15	**LASER treatment** UV curing of hybrid acryl-amide titania films spin-coated onto rigid substrates, Formation of localized wrinkled strips via localized UV light illumination and successive deposition of thin film material	Si, Silica	Acrylamide-titania	Not reported	No	1D ordered, 2D array, and disordered isotropic wrinkles	Gratings	[28]
16	**LASER treatment** Deposition of Chalcogenide thin films on Si substrates through magnetron sputtering, Wrinkle formation through focused pulsed LASER beam irradiation on rotating sample surface	Si	GeTe, $Ge_{30}Te_{70}$, $Ge_2Sb_2Te_5$	Not reported	No	Disordered isotropic labyrinthine wrinkles	Anti-counterfeiting tags	[29]
17	**LASER treatment** Wrinkle formation through LASER irradiation	PDMS	-	Cracks	No	Partially ordered 1D sinusoidal wrinkles	Not shown	[30]
18	**UV treatment** Wrinkle formation through UV induced gradient cross-linking and photochemical boundary		Anthracene containing PSPU and Graphene	No	No	Disordered labyrinthine wrinkles, different 2D patterned wrinkles	NIR controlled optical gratings	[31]
19	**UV treatment+ Thermally** Spin-coating PMMA on PDMS substrates followed by heating and cooling, Formation of wrinkle patterns under UV radiation or thermal stimulation of PMMA films	PDMS	PMMA	No	No	Disordered labyrinthine wrinkles	Tunable UV/thermal sensitive optical diffusers	[32]
20	**Thermally** Heating of multilayer system to a temperature higher than the T_g of second layer and lower than that of the uppermost layer, Formation of wrinkles through compressive stress generation	Si	PS/Al/P4VP	No	No	Isotropic disordered labyrinthine wrinkles	Estimation of T_g of polymeric thin films	[33]

682

683

Sl No.	Thin film processing technique	Substrate	Thin film material	Defects formed	Calibrated with respect to structure causing stimuli	Type of structures formed	Applications	Reference
21	**Thermally** Thermal evaporation of Al thin films on PS films spin-coated on Si wafers, Wrinkle formation on Al films through thermal annealing for atleast 3600s at temperatures above the glass transition temperature of PS	Si	PS/Al	Not reported	No	Isotropic disordered wrinkles	Estimation of stress-relaxation modulus of polymer thin films confined by both a substrate and a superstrate	[34]
22	**Thermally** Supersonic cluster beam implantation of neutral Au nanoparticles into thermally retractable PS sheets, Wrinkle formation through thermal shrinking of the material at 160°C for 6 minutes	PS sheet	Au nanoparticles	Not reported	No	Isotropic, Disordered 3D,2D and 1D wrinkles	Not shown	[35]
23	**Thermally** Spin-coating PAN solution on CNT-PDMS substrate followed by sequential exposure to UV light through photomask, Deposition of metal films on PAN layer through e-beam evaporation, Wrinkle formation in metal films through heat treatment	CNT-PDMS	PAN interlayer, Functional metallic layer of Al or Ge or Au	Not reported	No	1D,2D ordered sinusoidal strips wrinkles	Smart displays, devices for resolving light pollution	[36]
24	**Thermally** Dip-coating borosilicate glass substrate in ZnO sol gel, Heat treatment at 150°C in IR chamber of dip coater, Post annealing in air at 450°C for 1 hour, Multi layers prepared through the same procedure leading to wrinkle formation	Boro-silicate glass	ZnO	No	No	Isotropic labyrinthine wrinkles	Enhancing photocatalytic degradation of organic pollutants in water	[37]

Sl No.	Thin film processing technique	Substrate	Thin film material	Defects formed	Calibrated with respect to structure causing stimuli	Type of structures formed	Applications	Reference
25	**<u>Thermally</u>** Spin-coating PDMS on glass,Thermal evaporation of Al thin films on PDMS, enhancement of cross-linking in the PDMS due to the temperature of the film leading to freezing of patterns substrate and consequent wrinkling in thin film	PDMS	Al	Not reported	No	Disordered labyrinthine wrinkles	Fabrication of surfaces with controlled wettability and reflectance	[38]
26	**<u>Nanoimprint lithography and dewetting</u>** Soft lithography to imprint a PDMS mask onto a thermoplastic or sol-gel layer via nanoimprinting. Thermal deposition of thin layer of Chalcogenide glass followed by thermal annealing at different temperatures	Thermoplastic, Sol-gel	$Ge_6Se_{82}Te_{12}$, Se	Not reported	Yes	Dewetted droplets on patterned substrates	Metasurfaces and stretchable optics	[39]
27	**<u>Thermal deposition</u>** Thermal evaporation of thin films on flexible substrates	PDMS	Ga	No	Yes	Ga droplets on PDMS substrates	Mechanochromic sensors	[40]
28	**This paper:** **<u>Thermally</u>** Spin-coating PDMS solution on patterned Si mold followed by curing at 80°C for different time durations (ranging from 1hr to 6 hours), Peeling off the PDMS substrate and thin film deposition on its surface, Wrinkle formation in thin films through thermal heating for 3 minutes and subsequent cooling	PDMS 5, PDMS 10 of different softnesses	As_2Se_3, Al, Ag, PMMA (encompassing a wide range of materials like chalcogenide glasses, metals and polymers)	No	Yes (Periodicity d as a function of Change in temperature ΔT, also an equation illustrating the critical length required for ordered wrinkle formation in case of thermally induced wrinkles)	Ordered 1D sinusoidal, Ordered 2D zigzag, Disordered labyrinthine	Multilevel hybrid encryption device, Large area flexible reflective displays, dynamically tunable diffraction grating and optical diffusers, devices for increasing the out-coupling efficiency of encapsulated light sources, adaptive visible camouflage, mechanochromic sensors for healthcare	Novelty: (i) For the first time, this thermal process has been calibrated based on the wrinkle-inducing factors such as temperature change (ΔT), material properties like thermal expansion coefficients, and surface energy. This has led to the development of equations that aid in achieving customized wrinkle patterns with different thin films and substrates. (ii)Obtained large area, defect free,

								ordered and reversible wrinkles on metals, chalcogenides and polymers through a simple thermal processing technique (iii) Elaborately studied the effect of substrate softness on the formation of different thin film **surface morphologies**.

Table 2|Comparison of our work with existing works on wrinkles

5.2 Novelty in the Encryption device:

Our fabricated encryption device is a combination of software and hardware thereby providing complete protection from data theft and data tampering. It also boasts an exceptionally low decryption probability of the order of $\sim 10^{-53}$. Here is a comparison of our device with all similar reported works:

Sl. no.	Working principle	Possible states & levels of encryption	Maximum number of possible combinations (n= number of pixels)	Dynamic tunability	Reference
1.	**Encryption of 2D patterning through photo-induced gradient cross-linking and subsequent stretching and releasing for wrinkle formation. Wrinkle disappearance through thermal heating**	**i. 2 orientations: stretched & unstretched**	$C = 2$	**No (A pattern once printed cannot be changed)**	[41]
2.	**Disordered labyrinthine wrinkles acting as unique identifiers**	**i. 3 distinct color states of fluorescence**	$C = 3$	**No. Disordered labyrinthine wrinkle formations are unpredictable**	[42]
3.	**2D patterns of microarrays fabricated through multi-stage photo-patterning. Optical encryption by modulation of structural colors and FL/CPL through interferometric retroreflection and chemical treatment**	**i. 4 distinct orientations of microarrays ($\beta = 0°, 45°, 90°, 135°$)**	$C = 4$	**No (A pattern once printed cannot be changed)**	[43]

Sl. no.	Working principle	Possible states & levels of encryption	Maximum number of possible combinations (n= number of pixels)	Dynamic tunability	Reference
4.	Encryption through UV treatment and heating on thermochromic perovskite microcapsules (TPMs), perovskite QD microcapsules, and dye microcapsules	i. State of UV treatment ii. State of heating	$C = 4$	No	[44]
5.	Encryption based on cascaded encrypted LC elements by leveraging Malu's law in cascaded LC elements and the rotational degeneracy of LC molecules	i. 5(1 far field image and 4 near field images based on the relative orientation of the LC elements	$C = 5$	Not mentioned explicitly	[45]
6.	Encryption in bilayer systems by IR detection, temperature dependence, and visible anti-counterfeiting	i. Concentration of W-doped VO2 (determines 0/1 above a particular temperature ii. Presence and absence of structural colors in PS photonic crystals	$C = 2 \times 2^n$ $n = 16,\ C \cong 10^5$ $n = 36,\ C \cong 10^{11}$	No	[46]
7.	RH and LH polarized plasmonic chiral nanostructures arranged in definite orders give a uniqueness to the data through a distinctive g-factor as compared to the background	i. 3 states (2 polarization states LH and RH and 1 non-polarized state)	$C = 3^n$ $n = 16,\ C \cong 10^7$ $n = 36,\ C \cong 10^{17}$	No	[47]
8.	Optical encryption through controllable structural colors and polarization phases	i. 5 distinct color states	$C = 5^n$ $n = 16,\ C \cong 10^{11}$ $n = 36,\ C \cong 10^{25}$	No (A pattern once printed cannot be changed)	[48]

691

Sl. no.	Working principle	Possible states & levels of encryption	Maximum number of possible combinations (n= number of pixels)	Dynamic tunability	Reference
9.	Encryption through mechanical stretching of chiral liquid crystal elastomers of varying thicknesses	i. 7 color states	$C = 7^n$ $n = 16,\ C \cong 10^{13}$ $n = 36,\ C \cong 10^{30}$	No (Absence of calibration equation relating stimuli and the encryption parameters)	49
10.	Encryption through fluorescence, CPL, color emission and time response characteristics	i. 11 color states (including 1 colorless state)	$C = 11^n$ $n = 16,\ C \cong 10^{16}$ $n = 36,\ C \cong 10^{37}$	Not mentioned explicitly	50
11.	Encryption through dynamic PUF using a combination of transient fluorescence through QDs and temporally dependent luminescence	i. 9 color states for barcodes ii. 10 number states and 3 color states for each digital number	$C = 30^n$ $n = 16,\ C \cong 10^{23}$ $n = 36,\ C \cong 10^{53}$	Not mentioned explicitly	51
12.	Encryption through hybrid mode (software + hardware). Each pixel needs to be heated to a certain temperature (known only to intended receiver) and cooled down to room temperature for wrinkle formation. Upon reaching the room temperature each pixel has to be scanned under a microscope and their dimensions and wrinkle periodicities need to be entered in the software in the right order (known only to the intended receiver) for information decryption	i. Specific order of arrangement of lengths$(n!)$ ii. Specific order of arrangement of widths $(n!)$ iii. 7 possible temperature information for each pixel iv. Specific order of arrangement of breadths $(n!)$	$C = n! \times n! \times 7^n \times n!$ $n = 16,\ C \cong 10^{53}$ $n = 36,\ C \cong 10^{155}$	Yes (If the arrangement orders or wrinkle periodicities get leaked, the app can be stopped from launching and a different set of arrangement orders and temperatures can be used on the same device)	This device

Table 3|Comparison of our work with similar existing works on encryption devices

The salient novelty accompanying the fabrication process, materials used, calibration of the process and photonic applications, summarized from above discussion are as follows:

1) ***Simple fabrication process***: The processing technique involves thin film deposition on PDMS substrates followed by simple heating and subsequent cooling, thus marking a departure from the previous reliance on intricate chemical, mechanical and lithographic methods and making it highly scalable and cost effective.

2) ***Large area, cost-effective process:*** The process has been thoroughly studied and engineered to get large area ($\sim 100 cm^2$) ordered wrinkled samples that are almost free of defects like cracks and delaminations. Such large area flexible and stretchable defect free structures are crucial for applications in the domains of AR-VR due to their lightweight nature, uniform light scattering and ability to generate dynamically tuneable vivid structural colours, reducing dependence on traditional pigments and dyes for colour generation.

3) ***Impact in processing of micro and nanostructures*****:** For the first time, this thermal process has been calibrated based on the wrinkle-inducing factors such as temperature change (ΔT), material properties like thermal expansion coefficients, and surface energy. This has led to the development of equations that aid in achieving customized wrinkle patterns, thereby addressing a theoretical gap in this area.

4) ***Impact in the domain of soft materials:*** The process has been extensively studied to investigate how substrate softness influences the formation of different thin-film surface morphologies, thus impacting the thermal properties, optical behaviour, and functional performance of the materials in applications such as flexible electronics, biomaterials, and soft robotics.

5) ***Compatibility with different materials:*** Our method is compatible with a wide range of materials including metals, semiconductors and polymers. For the first time, we have achieved large area ordered wrinkles in Chalcogenide thin films.

6) ***Applications in encryption-decryption, soft photonics, healthcare and large-area smart displays:*** The applications of the thermo- and mechanoresponsive structures range from healthcare to dynamically tunable photonics, and optical devices. The fabricated multilevel hybrid encryption-decryption device can find great utility in military and government settings. The large-area flexible reflective displays, known for their energy efficiency and durability, are suited for use in electronic paper, outdoor advertising, wearable devices, and military settings. The thermo responsive large area ordered wrinkled structures also act as dynamically tunable diffraction gratings and adaptive visible camouflage that can find applications in military settings.

7) ***Applications in stretchable electronics domain:*** The fabricated thin film samples can find applications in stretchable interconnects, energy storage devices like flexible batteries and supercapacitors, as flexible substrates for OLEDs, photovoltaics and light-emitting diodes due to their light weight, dynamically tunable and high surface area, mechanical durability and ability to maintain electrical conductivity under deformation.

8) ***Applications in bioengineering and bio-interface sciences:*** The controlled thin film structures can also find applications in tissue engineering, cell studies involving mechanobiology, bio-sensing platforms, microfluidics, biomedical implants and artificial skins due to their dynamically tunable topographies and adhesion for guiding cell alignment, proliferation and specific interactions with biological samples. They can also act as reservoirs and carriers for controlled drug release. The

controlled patterns and high surface area offered by these structures are also beneficial for protein binding.

6. References

1. Müller, A., Wapler, M. C. & Wallrabe, U. A quick and accurate method to determine the Poisson's ratio and the coefficient of thermal expansion of PDMS. *Soft Matter* **15**, 779–784 (2019).

2. Zmrhalová, Z., Pilný, P., Svoboda, R., Shánělová, J. & Málek, J. Thermal properties and viscous flow behavior of As2Se3 glass. *J Alloys Compd* **655**, 220–228 (2016).

3. Málek, J. & Shánělová, J. Structural relaxation of As2Se3 glass and viscosity of supercooled liquid. *J Non Cryst Solids* **351**, 3458–3467 (2005).

4. Shchurova, T. N. & Savchenko, N. D. *Defense Technical Information Center Compilation Part Notice CORRELATION BETWEEN MECHANICAL PARAMETERS FOR AMORPHOUS CHALCOGENIDE FILMS*. *Journal of Optoelectronics and Advanced Materials* vol. 3 (2001).

5. Mel'Nichenko, T. D. *et al.* On the approximate estimation of the surface tension of chalcogenide glass melts. *Glass Physics and Chemistry* **35**, 32–42 (2009).

6. Fang, W. & Lo, C.-Y. *On the Thermal Expansion Coefficients of Thin Films*. *Sensors and Actuators* vol. 84 www.elsevier.nlrlocatersna (2000).

7. Samad, M. I. A. *et al.* Aluminium Thin Film Surface Modification via Low-Pressure and Atmospheric-Pressure Argon Plasma Exposure. *Journal of Surface Investigation* **16**, 421–426 (2022).

8. Lim, Y. Y., Chaudhri, M. M. & Enomoto, Y. Accurate determination of the mechanical properties of thin aluminum films deposited on sapphire flats using nanoindentations. *J Mater Res* **14**, 2314–2327 (1999).

9. Zoo, Y., Adams, D., Mayer, J. W. & Alford, T. L. Investigation of coefficient of thermal expansion of silver thin film on different substrates using X-ray diffraction. *Thin Solid Films* **513**, 170–174 (2006).

10. Oje, A. I., Ogwu, A. A., Mirzaeian, M., Oje, A. M. & Tsendzughul, N. Silver thin film electrodes for supercapacitor application. *Appl Surf Sci* **488**, 142–150 (2019).

11. Laugier, M. *Letter Determination of Young's Modulus in Vacuum-Evaporated Thin Films of Aluminium and Silver*. *Thin Solid Films* vol. 75 (1981).

12. Han, G., Huan, S., Han, J., Zhang, Z. & Wu, Q. Effect of acid hydrolysis conditions on the properties of cellulose nanoparticle-reinforced polymethylmethacrylate composites. *Materials* **7**, 16–29 (2014).

13. Mounder Kouicem, M. *et al.* An investigation of adhesion mechanisms between plasma-treated PMMA support and aluminum thin films deposited by PVD. (2021) doi:10.1016/j.apsusc.2021.150322ï.

14. Yan, Z. *et al.* Floating solid-state thin films with dynamic structural colour. *Nat Nanotechnol* **16**, 795–801 (2021).

15. Zeng, S. *et al.* Bio-inspired sensitive and reversible mechanochromisms via strain-dependent cracks and folds. *Nat Commun* **7**, (2016).

16. Li, Z. *et al.* Harnessing Surface Wrinkling–Cracking Patterns for Tunable Optical Transmittance. *Adv Opt Mater* **5**, (2017).

17. Lipomi, D. J. *et al.* Skin-like pressure and strain sensors based on transparent elastic films of carbon nanotubes. *Nat Nanotechnol* **6**, 788–792 (2011).

18. Stafford, C. M. *et al.* A buckling-based metrology for measuring the elastic moduli of polymeric thin films. *Nat Mater* **3**, 545–550 (2004).

19. Takeshima, T. *et al.* Photoresponsive Surface Wrinkle Morphologies in Liquid Crystalline Polymer Films. *Macromolecules* **48**, 6378–6384 (2015).

20. Gabardo, C. M. *et al.* Rapid prototyping of all-solution-processed multi-lengthscale electrodes using polymer-induced thin film wrinkling. *Sci Rep* **7**, (2017).

21. Chung, J. Y., Chastek, T. Q., Fasolka, M. J., Ro, H. W. & Stafford, C. M. Quantifying residual stress in nanoscale thin polymer films via surface wrinkling. *ACS Nano* **3**, 844–852 (2009).

22. Lin, R., Qi, Y., Kou, D., Ma, W. & Zhang, S. Bio-Inspired Wrinkled Photonic Elastomer with Superior Controllable and Mechanically Stable Structure for Multi-Mode Color Display. *Adv Funct Mater* **32**, (2022).

23. Yang, S., Khare, K. & Lin, P. C. Harnessing surface wrinkle patterns in soft matter. *Adv Funct Mater* **20**, 2550–2564 (2010).

24. Zeng, S. *et al.* Moisture-Responsive Wrinkling Surfaces with Tunable Dynamics. *Advanced Materials* **29**, (2017).

25. Yang, Y. & Zhao, H. Water-induced polymer swelling and its application in soft electronics. *Appl Surf Sci* **577**, (2022).

26. Chung, J. Y., Nolte, A. J. & Stafford, C. M. Diffusion-controlled, self-organized growth of symmetric wrinkling patterns. *Advanced Materials* **21**, 1358–1362 (2009).

27. Xie, J., Han, X., Zong, C., Ji, H. & Lu, C. Large-area patterning of polyaniline film based on in situ self-wrinkling and its reversible doping/dedoping tunability. *Macromolecules* **48**, 663–671 (2015).

28. Takahashi, M. *et al.* Photoinduced formation of wrinkled microstructures with long-range order in thin oxide films. *Advanced Materials* **19**, 4343–4346 (2007).

29. Martinez, P. *et al.* Laser Generation of Sub-Micrometer Wrinkles in a Chalcogenide Glass Film as Physical Unclonable Functions. *Advanced Materials* **32**, (2020).

30. Qi, L. *et al.* Writing Wrinkles on Poly(dimethylsiloxane) (PDMS) by Surface Oxidation with a CO2 Laser Engraver. *ACS Appl Mater Interfaces* **10**, 4295–4304 (2018).

31. Yuan, W. *et al.* Photochemical Design for Diverse Controllable Patterns in Self-Wrinkling Films. *Advanced Materials* **36**, (2024).

32. Jiang, S., Yin, X., Bai, J., Yu, B. & Qian, L. Fabrication of ultraviolet/thermal-sensitive PMMA/PDMS wrinkle structures and the demonstration as smart optical diffusers. *Ceram Int* **49**, 10787–10794 (2023).

33. Yoo, S. S. *et al.* Cumulative energy analysis of thermally-induced surface wrinkling of heterogeneously multilayered thin films. *Soft Matter* **14**, 704–710 (2018).

34. Chan, E. P., Kundu, S., Lin, Q. & Stafford, C. M. Quantifying the stress relaxation modulus of polymer thin films via thermal wrinkling. *ACS Appl Mater Interfaces* **3**, 331–338 (2011).

35. Greco, F. *et al.* Conducting shrinkable nanocomposite based on au-nanoparticle implanted plastic sheet: Tunable thermally induced surface wrinkling. *ACS Appl Mater Interfaces* **7**, 7060–7065 (2015).

36. Chen, S. *et al.* Dynamic metal patterns of wrinkles based on photosensitive layers. *Sci Bull (Beijing)* **67**, 2186–2195 (2022).

37. Daher, E. A., Riachi, B., Chamoun, J., Laberty-Robert, C. & Hamd, W. New approach for designing wrinkled and porous ZnO thin films for photocatalytic applications. *Colloids Surf A Physicochem Eng Asp* **658**, (2023).

38. Das, A., Banerji, A. & Mukherjee, R. Programming Feature Size in the Thermal Wrinkling of Metal Polymer Bilayer by Modulating Substrate Viscoelasticity. *ACS Appl Mater Interfaces* **9**, 23255–23262 (2017).

39. Das Gupta, T. *et al.* Self-assembly of nanostructured glass metasurfaces via templated fluid instabilities. *Nat Nanotechnol* **14**, 320–327 (2019).

40. Sahu, R. R. *et al.* Single-step fabrication of liquid gallium nanoparticles via capillary interaction for dynamic structural colours. *Nat Nanotechnol* **19**, 766–774 (2024).

41. Wen, T. *et al.* Phase-transition-induced dynamic surface wrinkle pattern on gradient photo-crosslinking liquid crystal elastomer. *Nature Communications* **15**, (2024).

42. Ma, T. *et al.* Dynamic wrinkling pattern exhibiting tunable fluorescence for anticounterfeiting applications. *Nat Commun* **11**, (2020).

43. Feng, Z. *et al.* Dynamic multimodal information encryption combining programmable structural coloration and switchable circularly polarized luminescence. *Nat Commun* **16**, 2264 (2025).

44. Yuan, X. *et al.* Multilevel Information Encryption Based on Thermochromic Perovskite Microcapsules via Orthogonal Photic and Thermal Stimuli Responses. *ACS Nano* **18**, 10874–10884 (2024).

45. Xu, X. *et al.* Optical Information Encryption Based on Secret Sharing Liquid Crystal Elements with Spatial Dislocation. *Laser Photon Rev* (2024) doi:10.1002/lpor.202400168.

46. Wang, J. *et al.* Multilevel Information Encryption Mediated by Reconfigurable Thermal Emission in Smart Bilayer Material. *Laser Photon Rev* **18**, (2024).

47. Lee, Y. H. *et al.* Hierarchically manufactured chiral plasmonic nanostructures with gigantic chirality for polarized emission and information encryption. *Nat Commun* **14**, (2023).

48. Li, L. Y., Tan, Q. W., Wang, X. L., Wang, Y. Z. & Song, F. Bioinspired Hierarchical Photonic Structures with Controllable Polarization and Color for Optical-Multiplexed Information Encryption. *ACS Nano* (2025) doi:10.1021/acsnano.4c16597.

49. Nam, S., Woo, S., Park, J. Y. & Choi, S. S. Programmable optical encryption using thickness-controlled stretchable chiral liquid crystal elastomers. *Light Sci Appl* **14**, (2025).

50. Lin, S. *et al.* Photo-triggered full-color circularly polarized luminescence based on photonic capsules for multilevel information encryption. *Nat Commun* **14**, (2023).

51. Chen, H. *et al.* Dynamic Anti-Counterfeiting Labels with Enhanced Multi-Level Information Encryption. *ACS Appl Mater Interfaces* **15**, 2104–2111 (2023).